

# Upper mantle and lithospheric heterogeneities in central and eastern Europe as observed by teleseismic receiver functions

Wolfram H. Geissler,<sup>1\*</sup> Rainer Kind<sup>1,2</sup> and Xiaohui Yuan<sup>1</sup>

<sup>1</sup>GeoForschungsZentrum Potsdam, Telegrafenberg, 14473 Potsdam, Germany. E-mail: Wolfram.Geissler@awi.de

<sup>2</sup>Freie Universität Berlin, Germany

Accepted 2008 February 22. Received 2008 February 22; in original form 2007 August 7

## SUMMARY

Data from 90 permanent broad-band stations spread over central and eastern Europe were analysed using Ps receiver functions to study the crustal and upper-mantle structure down to the mantle transition zone. Receiver functions provide valuable information on structural features, which are important for the resolution of European lithospheric dynamics. Moho depths vary from less than 25 km in extensional areas in central Europe to more than 50 km at stations in eastern Europe (Craton) and beneath the Alpine–Carpathian belt. A very shallow Moho depth can be observed at stations in the Upper Rhine Graben area (*ca.* 25 km), whereas, for example, stations in the SW Bohemian Massif show a significantly deeper Moho interface at a depth of 38 km.  $V_p/V_s$  ratios vary between 1.60 and 1.96, and show no clear correlation to the major tectonic units, thus probably representing local variations in crustal composition. Delayed arrivals of converted phases from the mantle transition zone are observed at many stations in central Europe, whereas stations in the cratonic area show earlier arrivals compared with those calculated from the IASP91 Earth reference model. Differential delay times between the P<sub>410s</sub> and P<sub>660s</sub> phases indicate a thickened mantle transition zone beneath the eastern Alps, the Carpathians and the northern Balkan peninsula, whereas the transition zone thickness in eastern and central Europe agrees with the IASP91 value. The thickening of the mantle transition zone beneath the eastern Alps and the Carpathians could be caused by cold, deeply subducted oceanic slabs.

**Key words:** Mantle processes; Composition of the mantle; Phase transitions; Cratons; Crustal structure; Europe.

## 1 INTRODUCTION

Knowledge of the deep seismic and thermal structure of the earth's crust, together with its composition as far down as the upper mantle and the mantle transition zone, is important in understanding the geodynamic history of Europe. In surface geology, there exist huge differences between the Pre-Cambrian East European Craton (EEC), the Palaeozoic platform of central Europe, and the recently active collision zone of the Alpine–Carpathian orogenic system (e.g. Banka *et al.* 2002; Fig. 1). However, it is still unclear how deeply the origins of these different tectonic units and related processes penetrate the upper mantle.

The EEC, finally consolidated in the late Precambrian, is divided from the rest of Europe by the Transeuropean Suture Zone (TESZ), which runs from the North Sea in the northwest to the Black Sea in the southeast. The TESZ is commonly split into the Tornquist–Teisseyre (TTZ) and Sorgenfrei–Tornquist zones (STZ). The Thor

Suture is generally interpreted as a thrust of Caledonian nappes on Baltica (EEC). The basement of central Europe was mainly consolidated after the Caledonian (early Palaeozoic) and Variscan (Late Palaeozoic) orogenies. During the Mesozoic, central Europe was further consolidated and covered by platform sediments. Its southern periphery was influenced by the rifting and opening of the Tethys Ocean. During the late Mesozoic and Cainozoic, the study area southwest of the TESZ was influenced strongly by the Alpine orogeny and rifting in the North Atlantic. The Alpine–Carpathian belt is a result of the Tertiary African–European convergence and of the closure of the Tethys ocean, associated with the collision of several microplates with the European plate (e.g. Nemcok *et al.* 1998; Sperner *et al.* 2001; Seghedi *et al.* 2005). Within the central Alps (Austrian, Swiss), subduction of the central European lithosphere is observed towards the south (e.g. TRANSALP Working Group 2002; Lueschen *et al.* 2006). In the Carpathians, subduction is (was) mostly directed towards the Pannonian basin (e.g. Sperner *et al.* 2001).

The palaeotemperature distribution and composition of the deep lithosphere can be constrained by xenolith studies and exhumed slivers of mantle rocks. Unfortunately, outcrops of these rocks are

\*Now at: AWI Bremerhaven, Am Alten Hafen 26, 27568 Bremerhaven, Germany.

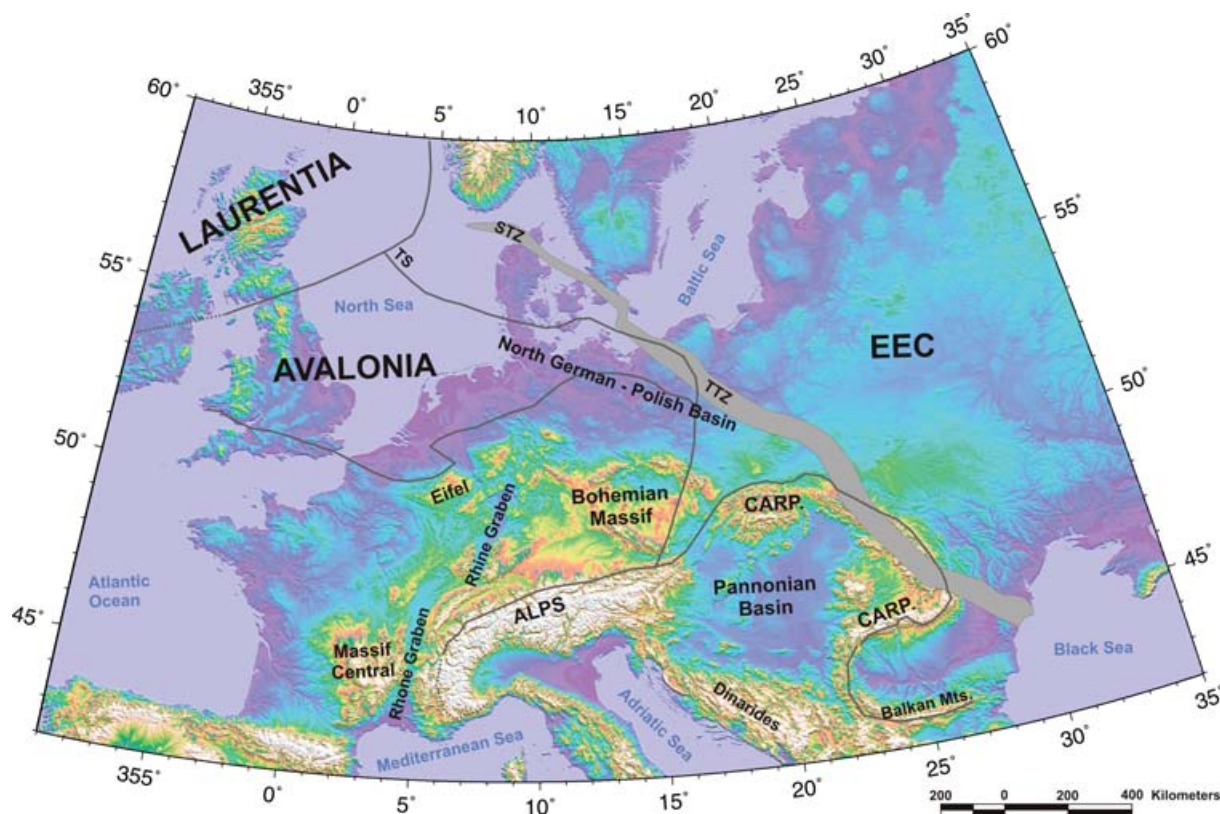


**Figure 1.** Topographic map of Europe with simplified tectonic elements of Europe after Banka *et al.* (2002). Carp., Carpathians; EEC, East European Craton, STZ, Sorgenfrei–Tornquist zone; TTZ, Tornquist–Teisseyre zone; TS, Thor suture.

scarce, both in time and space. They provide information only very locally, whereas geophysical methods can study the recent temperature distribution and compositional variations over broader areas. As identified in previous studies, there exist large differences in several geophysical fields between central and eastern Europe across the TESZ. Gravity studies first revealed the strong differences between the old core of Europe (EEC) and the Palaeozoic to recent mobile belts in the SW (Caledonian, Variscan and Alpine belts) (Tornquist 1908; Yegorowa & Starostenko 1999). Artemieva (2003) found that the uppermost mantle beneath the EEC is up to 1.6 per cent less dense than it is beneath central Europe. Strong anomalies in the distribution of seismic velocities were found by tomography and surface wave studies (e.g. Zielhuis & Nolet 1994; Meier *et al.* 1997; Ritzwoller *et al.* 2002; Shapiro & Ritzwoller 2002). Goes *et al.* (2000) calculated temperature differences of up to 300 K in the uppermost mantle using seismic velocities, under the assumption that these velocities depend more on temperature than on compositional variations. Using traveltimes tomography, Wortel & Spakman (2000), Piromallo *et al.* (2001) and Piromallo & Facenna (2004) found evidence for high  $P$ -wave velocities in the mantle transition zone at depths from 500 to 600 km beneath the Alpine–Carpathian belt and the Mediterranean Sea. These high seismic velocities were interpreted as being caused by cold, deeply subducted material.

One possible method for studying temperature variations at the bottom of the upper mantle is to analyse the variations in the seismic discontinuities of the mantle transition zone at depths of about 410 and 660 km. It is now widely accepted that most of the discontinuities in velocity and density at these depths are the result of phase changes in olivine and other minerals (e.g. Vacher *et al.* 1998;

Helfrich & Wood 2001; Lebedev *et al.* 2002, 2003). The transformation of the olivine component has a major impact on the seismic velocities observed. Olivine is transformed to a spinel structure at a depth of about 410 km and finally breaks down to perovskite and magnesiowüstite at about 660 km (e.g. Helfrich & Wood 2001). Both transformations are temperature-dependent but have opposing Clapeyron slopes (e.g. Fei *et al.* 2004; Katsura *et al.* 2004). If the temperature is increased (e.g. in a plume environment), then the transformation normally observed at 410 km should be found at a deeper level, and the one observed at 660 km should be found at a shallower level. The opposite holds true for a temperature decrease as it can be expected in subduction environments.

SS precursor and the  $P_s$  receiver function studies are the most common techniques used to study discontinuities of the mantle transition zone (Lawrence & Shearer 2006). Using a SS precursor study, Gossler & Kind (1996) found a transition zone that was 14 km thicker beneath continents than beneath oceans. According to Shearer (2000), the topography of the upper-mantle seismic discontinuities at 410 and the 660 km seem to be largely unrelated at a global scale, with the 660 topography exhibiting significantly larger variations in peak-to-peak amplitude than the 410 topography. However, Li *et al.* (2003a) and Chevrot *et al.* (2000) found that the delay times of  $P_s$ -converted 410 and 660 phases are generally quite well correlated, which implies that most of the variations in delay time can be attributed to variations in upper-mantle seismic velocity. Assuming a more or less homogenous transition zone, its thickness  $d_{TZ}$  can be determined more reliably than the individual depths of the 410 and 660 km discontinuities. The sharpness of the 410 and 660 km discontinuities could be 5 km or less as estimated

from short period P'P' precursors (Benz & Vidale 1993). There is still some disagreement over the existence of a detectable seismic discontinuity (enhanced velocity gradient) at a depth of about 520 km (Shearer 1990).

In this paper, we apply the Ps receiver function method to study the upper mantle down to the mantle transition zone at the contact of the Precambrian lithosphere in eastern Europe and the Palaeozoic-to-recently consolidated central Europe, including large parts of the Alpine–Carpathian orogenic belt.

## 2 METHOD

The Ps receiver function method is a widely accepted approach for studying lithospheric and upper-mantle seismic discontinuities. Our analysis of teleseismic broad-band recordings follows the work of Vinnik (1977), Kind *et al.* (1995, 2000) and Yuan *et al.* (1997). Rotation from the Z, N–S and E–W (ZNE) components into the P, SV and SH system (LQT components) is used to separate different wave types. For the rotation of the horizontal components, in most cases we used theoretical values of backazimuth calculated from the coordinates of the event and the station. The values thus obtained commonly differ by less than 10 degrees from the observed ones. However, at stations in orogens, such as the Alps and Carpathians, the backazimuth deviations are significantly larger. In such cases, the backazimuth was estimated from polarization analysis of the horizontal components. Generally, the angles of incidence were determined by minimizing the energy on the SV component ( $Q$ ) at the time of the  $P$  signal. This was achieved by computing the eigenvalues of the covariance matrix of the  $P$  signal, following Kind *et al.* (1995).

We used a time-domain deconvolution method to remove the source signal and source-side reverberations from the records, in order to allow records from different events to be stacked. Amplitudes of the SV and SH components were normalized in relation to the incident  $P$  wave. Arrival times were measured at the maximum of the deconvolved  $P$ -wave signal. For moveout correction, the IASP91 Earth reference model (Kennett 1991) was used to reduce the time scale of records at any distance to the fixed reference epicentral distance of  $67^\circ$  (slowness:  $6.4 \text{ s deg}^{-1}$ ). This means stretching (or compressing) waveforms for events at larger (or shorter) distances, respectively. In this way, primary  $P$ -to- $S$  converted phases are aligned parallel to the  $P$  phase and multiple phases can be identified by their slowness difference (not parallel to the  $P$  phase). Moho depth and average crustal  $V_p/V_s$  ratios were analysed using crustal multiples (Zhu & Kanamori 2000).

In order to study the effect of lithospheric structure on the delay times of  $P_{410s}$  and  $P_{660s}$ , we analysed synthetic seismograms in the same way as the real data. The reflectivity method was used to compute the theoretical seismograms (Kind 1985).

## 3 DATA

We analysed teleseismic data from 90 permanent broad-band stations belonging to various seismic networks in central and eastern Europe (Fig. 2, Table 1). Most of the stations are equipped with STS-1 or STS-2 seismometers. Generally, we analysed hundreds of events at single stations, but for some stations less than 50 events could be used due to different reasons. At the stations of the Gräfenberg array (GRA1, GRB1 and GRC1) we analysed more than 1000 events

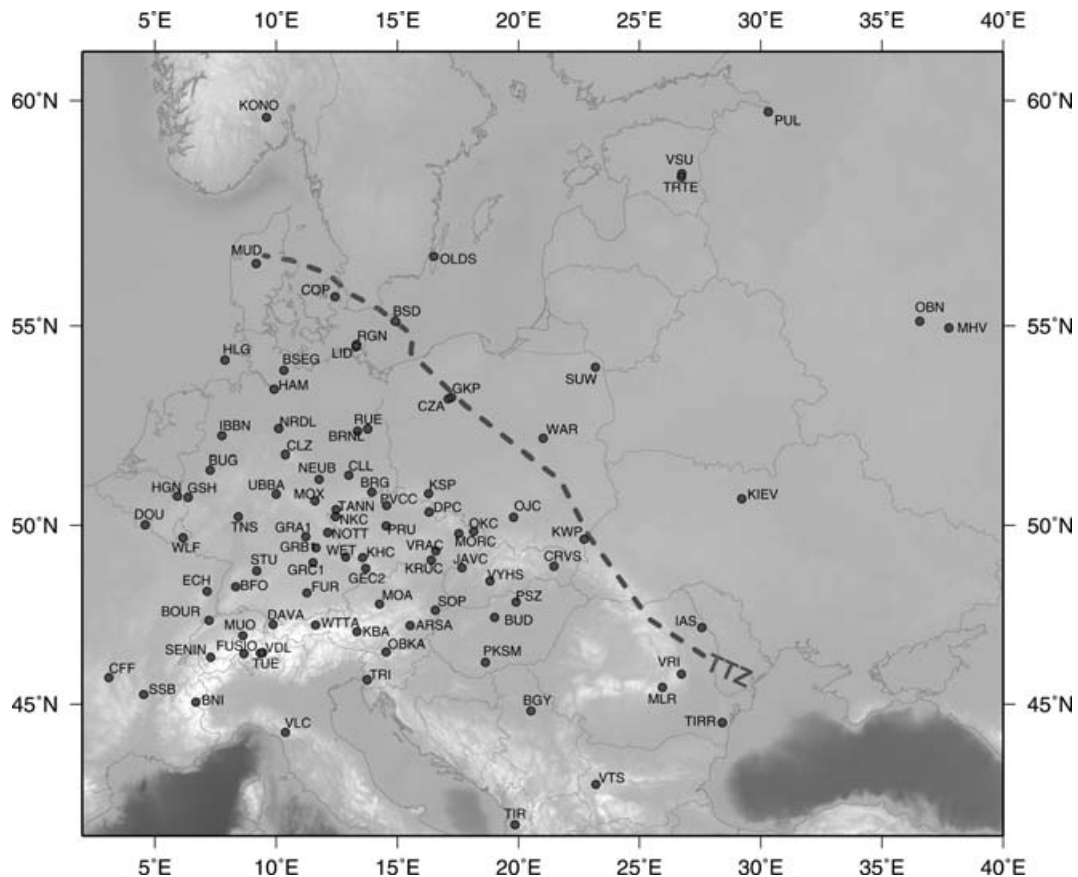


Figure 2. Distribution of the permanent seismic stations in central and eastern Europe that were used in this study.

**Table 1.** Station parameters, Moho Ps delay times  $t_{Ps}$ , amplitudes of Moho conversions relative to primary P wave ( $A$ ), Moho depth ( $H$ ) and  $V_p/V_s$  ratios obtained by the method of Zhu & Kanamori (2000), number of stacked traces  $n$ . The delay times of the  $P_{410s}$  and  $P_{660s}$  are given, as well as the differential delay times, the minimum signal-to-noise ratio of the  $P_{\text{moho}s}$  of stacked single traces (SNR-Moho), and the number of traces.

Station	Net	Lat [°N]	Lon [°E]	Elev. (m)	$t_{Ps}$ (Moho) (s)	$A_{\text{Moho}}$	$H$ (km)	$V_p/V_s$	$n$ (Moho)	$t_{P410s}$ (s)	$t_{P660s}$ (s)	$d_{t_{660-410}}$ (s)	SNR-Moho	$n$ (MTZ)
Czech Republic, Slovakia														
DPC	IG-CAS	50.350	16.322	748	3.7	0.09	28	1.82	478	44.3	69.1	24.8	1	459
NKC	IG-CAS	50.233	12.448	564	3.4	0.12	29	1.72	199	—	69.0	—	1	188
KHC	IG-CAS	49.131	13.578	700	4.4	0.08	38	1.71	264	44.7	68.5	23.8	1	252
PRU	IG-CAS	49.988	14.542	302	3.6	0.10	33	1.69	198	44.4	68.1	23.7	5	41
PVCC	IG-CAS	50.528	14.569	311	3.9	0.09	29	1.81	79	—	—	—	—	—
OKC	IG-CAS	49.838	18.147	272	4.1	0.08	32	1.77	209	—	69.4	—	1	202
MORC	IPE/GEOFON	49.776	17.546	740	4.2	0.04	32	1.81	472	45.0	70.7	25.7	5	66
JAVC	IPE/ZAMG	48.859	17.671	828	3.6	0.12	32	1.70	142	46.0	69.8	23.8	1	124
KRUC	IPE/ZAMG	49.062	16.395	341	3.7	0.07	31	1.66	144	44.4	68.5	24.1	1	125
VRAC	IPE	49.308	16.593	470	4.0	0.06	35	1.69	114	45.5	69.5	24.0	1	89
VYHS	SK	48.494	18.836	480	3.3	0.11	30	1.67	119	45.8?	71.3	25.5	1	100
CRVS	SK	48.902	21.461	476	3.6	0.04	31	1.74	117	—	—	—	—	—
Germany														
GRAI	GRF	49.692	11.222	500	3.7	0.10	32	1.73	1093	45.1	69.1	24.0	1	1072
GRB1	GRF	49.391	11.652	494	3.7	0.10	30	1.76	1001	44.0	68.1	24.1	1	980
GRC1	GRF	48.996	11.521	512	3.3	0.12	31	1.67	944	44.2	68.3	24.1	1	918
BFO	GRSN	48.330	8.330	589	3.0	0.11	27	1.69	534	43.7	68.2	24.5	1	512
BRG	GRSN	50.873	13.943	296	3.6	0.11	30	1.75	496	44.5	67.8	23.3	1	475
BRNL	GRSN	52.428	13.358	42	3.3	—	26?	—	229	45.2	68.2	23.0	5	60
BSEG	GRSN	53.935	10.317	40	4.6	0.16	33	1.86	241	—	—	—	—	—
BUG	GRSN	51.441	7.269	85	4.1	0.08	32	1.79	543	44.3?	68.2	23.9	9	43
CLL	GRSN	51.308	13.003	230	3.4	0.12	29	1.72	515	43.8	67.3	23.5	1	490
CLZ	GRSN	51.842	10.372	680	4.5	0.09	32	1.88	550	43.8	67.7	23.9	1	526
FUR	GRSN	48.163	11.275	565	4.3	0.13	31	1.88	533	—	—	—	—	—
GEC2	GERESS	48.845	13.702	1132	4.4	0.09	37	1.73	261	45.1	69.9?	24.8	1	288
GSH	GRSN	50.737	6.380	370	3.7	0.11	28	1.82	107	44.4	68.3	23.9	1	102
HAM	GRSN	53.465	9.925	30	4.0	0.09	31	1.82	151	—	—	—	—	—
HLG	GEOFON	54.185	7.884	41	3.8	0.18	32	1.73	134	44.9?	68.1	—	1	125
IBBN	GRSN	52.307	7.757	140	3.4	0.07	37	1.57	218	44.0	67.5	23.5	1	207
MOX	GRSN	50.645	11.616	455	3.5	0.11	30	1.72	528	44.1	68.4?	24.3	1	528
NEUB	W-Saxony	51.208	11.775	200	3.6	0.07	31	1.71	41	—	—	—	—	—
NRDL	GRSN	52.494	10.107	-355	2.5	0.15	20?	—	120	43.8	67.4	23.6	1	117
NOIT	Bavaria	49.811	12.123	470	3.4	0.10	31	1.69	98	45.6	69.3	23.7	1	95
RGN	GRSN	54.548	13.321	15	4.5	0.13	36	—	252	44.5	68.4	23.9	6	40
LID	GRSN	54.500	13.300	1	4.6	0.16	37	—	48	—	—	—	—	—
RUE	GEOFON	52.476	13.780	40	3.7	0.08	31	1.71	221	43.6	67.8	24.2	1	212
TANN	W-Saxony	50.415	12.461	836	3.5	0.08	27	1.75	45	43.0	67.8?	24.8	1	41
TNS	GRSN	50.223	8.447	815	2.9	0.11	24	1.76	500	45.8	69.4	23.6	1	471
STU	GEOFON	48.770	9.190	360	2.9	0.11	25	1.73	416	44.1	68.1	24.0	1	392

Table 1. (Continued.)

Station	Net	Lat [°N]	Lon [°E]	Elev. (m)	$t_{Ps}$ (Moho) (s)	$A_{Moho}$	$H$ (km)	$V_p/V_s$	$n$ (Moho)	$t_{P410s}$ (s)	$t_{P660s}$ (s)	$dt_{660-410}$ (s)	SNR-Moho	$n$ (MTZ)
UBBA	GRSN	50.819	10.001	-526	3.2	0.12	29	1.68	74	44.4	-	-	1	74
WET	GRSN	49.144	12.878	613	4.3	0.09	34	1.79	576	44.6	68.6	24.0	1	545
France, Benelux														
ECH	GEOSCOPE	48.216	7.158	580	3.0	0.09	26	1.70	377	44.2	68.7	24.5	1	354
SSB	GEOSCOPE	45.279	4.542	700	3.1	0.09	29	1.67	382	45.3	69.7	24.4	1	360
CFE	RENASS	45.762	3.102	400	3.5	0.12	27	1.81	33	-	-	-	-	-
HGN	KNMI	50.764	5.932	135	3.9	0.08	32	1.76	229	43.7	67.9	24.2	1	215
DOU	GEOSCOPE	50.005	4.595	224	4.9	0.09	35	1.84	37	-	-	-	-	-
WLF	GEOFON	49.665	6.152	295	3.8	0.14	25	1.94	426	45.0	68.3; 71.5	23.3?	1	411
Balkan, Romania														
VTS	GEOFON	42.600	23.200	1490	3.7	0.05	37	1.81	253	43.7	69.6	25.9	1	251
MLR	GEOFON	45.491	25.946	1378	6.1	0.07	45	1.81	302	42.3	68.3?	26.0	1	244
IAS	RO	47.193	27.562	160	4.4	0.10	34	1.82	33	-	-	-	-	-
VRI	RO	45.866	26.728	475	3.9	0.08	28 (46)	-; (1.54)	143	-	66.0	-	1	124
TIRR	GEOFON	44.458	28.413	77	3.8	0.10	37	1.71	132	44.1	68.8	24.7	1	133
TIR	MN	41.347	19.863	247	6.1	0.31	54	1.68	103	45.1	66.8; 70.0	-	2	73
BGY	MN	44.800	20.520	250	3.6	0.11	29	-	98	-	-	-	-	-
Poland, Baltic, Russia, Ukraine														
SUW	PL	54.013	23.181	152	5.6	0.12	41	1.84	290	43.1	67.2	24.1	1	228
KWP	PL	49.631	22.708	448	4.1	0.21	36	1.72	205	43.4	69.2?	25.8	1	202
CZA	PL	53.230	17.094	169	4.8	0.14	38	1.78	25	-	-	-	-	-
GKP	PL	53.270	17.237	115	4.4	0.09	26?; 39	1.75?; 1.67	73	43.5	69.5?	-	1	64
KSP	PL	50.840	16.290	353	4.0	0.06	30	1.83	131	44.4	68.4	24.0	1	109
OJC	PL	50.220	19.798	300	3.7	0.07	32	1.71	129	42.8?	67.3; 70.0	-	1	108
WAR	PL	52.242	21.024	110	4.0	0.13	43	1.59?	79	42.0	-	-	1	70
TRTE	GEOFON	58.379	26.721	100	5.2	0.08	43	1.74	167	42.0	65.9	23.9	1	125
VSU	GEOFON	58.462	26.735	63	5.2	0.08	43	1.75	122	42.4	65.9	23.5	1	97
PUL	GEOFON	59.767	30.317	65	6.1	0.09	48	1.78	178	41.9	65.7	23.8	1	171
KIEV	GSN-IU	50.694	29.208	124	5.0	0.09	34	1.89	251	42.5	66.6	24.1	1	239
OBN	GSN-II	55.114	36.569	130	5.3	0.07	49	1.61	561	43.2	66.8	23.6	1	554
MHV	GEOFON	54.958	37.767	150	5.6	0.07	48	1.60	323	42.9	66.7	23.8	1	321
Alps (Italia, Austria)														
BNI	MN	45.050	6.680	1410	6.2	0.08	48	1.79	233	45.9	68.8	22.9	1	227
TRI	MN	45.710	13.760	161	5.0	0.08	39	1.79	160	43.8	68.9; 72.6	25.1	1	124
TUE	MN	46.472	9.347	1924	4.1	0.13	31	1.83	140	44.2	67.3	23.1	1	141
VLC	MN	44.159	10.386	555	3.5	0.11	30	1.74	81	43.5?	67.6?	24.1	1	80
ARSA	OE	47.251	15.523	577	4.3	0.09	31	1.84	159	42.6; 45.9	72.7	-	1	139
DAVA	OE	47.287	9.880	1602	4.7	0.12	39	1.74	132	45.1	72.5?	-	1	123
WTTA	OE	47.264	11.636	1764	6.7	0.14	48	1.85	142	43.6	66.9	-	1	129

**Table 1.** (Continued.)

Station	Net	Lat [°N]	Lon [°E]	Elev. (m)	$t_{ps}$ (Moho) (s)	$A_{\text{Moho}}$	$H$ (km)	$V_p/V_s$	$n$ (Moho)	$t_{p410s}$ (s)	$t_{p660s}$ (s)	$d_{f660-410}$ (s)	SNR-Moho	$n$ (MTZ)
OBKA	OE	46.509	14.549	1075	5.6	0.09	46	—	144	43.3	66.9?; 69.2	25.9	2	90
MOA	OE	47.850	14.266	572	4.7	0.09	39	1.74	139	45.4?	69.9	—	1	137
KBA	OE	47.078	13.345	1721	5.2	0.06	42	—	138	46.1?	66.9	—	1	126
Hungary														
PSZ	GEOFON	47.918	19.894	940	3.4	0.11	30	1.70	249	41.6?; 47.1?	69.0	—	1	192
SOP	HU	47.683	16.558	260	3.7	0.11	27	1.82	146	44.0	68.2?	—	1	128
BUD	HU	47.484	19.024	196	4.0	0.07	28	1.68	117	45.4?	71.6	26.2	1	102
PKSM	HU	46.212	18.641	170	2.9	0.11	24	1.76	154	44.2	70.8?	26.6	3	89
Northern Europe														
COP	DK	55.685	12.433	13	4.1	0.11	27	1.96	90	44.5	68.2	—	2	52
MUD	DK	56.455	9.173	12	3.3	0.18	33	1.65	58	46.8?	67.7	20.9	1	54
BSD	DK	55.114	14.915	88	4.1	0.09	28	1.91	102	43.6	67.5	23.9	1	85
OLDS	TE	56.619	16.499	30	5.3	0.07	38	1.88	36	42.7	66.8	24.1	1	33
DSB	GEOFON	53.245	-6.376	236	3.3	0.09	32	1.67	212	44.2?	68.4?	—	2	130
ESK	GSN-II	55.317	-3.205	242	3.9	0.10	29	1.80	219	43.2	68.4?	—	1	211
KONO	ASRO	59.649	9.598	216	4.0	0.10	35	1.71	342	43.0	67.2	24.2	1	334
BORG	—	64.747	-21.327	110	3.6	0.05	9	1.85	89	48.5	73.5	25.0	1	86
KBS	GEOFON	78.920	11.920	77	3.4	0.11	25	1.87	182	43.2	67.5?; 70.1	—	1	169
Suisse														
BOURR	CH	47.395	7.231	860	3.3	0.08	30	1.70	151	44.8	69.2	24.4	1	103
FUSIO	CH	46.455	8.663	1480	4.5	0.09	37	—	145	—	68.5	—	1	86
MUO	CH	46.969	8.638	1920	4.3	0.11	29	1.91	155	46.7	69.1	22.4	1	99
SENIN	CH	46.363	7.299	2035	4.6	0.09	39	1.72	48	43.9	68.3	24.4	1	24
VDL	CH	46.485	9.451	1927	6.1	0.12	42	1.89	48	46.3	68.5	22.2	1	39
Mean					4.1	0.10	33	1.76		44.2	68.4	24.2		
$\sigma$					0.9	0.04	7	0.08		1.2	1.5	1.0		

Notes: Where  $H$  and  $V_p/V_s$  ratio could not be estimated,  $H$  was calculated using  $V_p/V_s = 1.73$ .

from 25 yr. Most data were filtered using a third-order Butterworth high-pass filter with a corner period of 50 s. At some stations in coastal regions and in sedimentary basins, we filtered the data using a corner period of 30 s. Furthermore, we performed filter tests to enhance the signals from the mantle transition zone. Good results were obtained using a 3 s low-pass filter. Only stations where similar arrival times were obtained using different filters were assumed to show reliable Ps conversions from the mantle transition zone. For the final determination of Ps conversion delay times, we used the high-pass filtered data. We also tested  $P_{410S}$  and  $P_{660S}$  arrivals for subgroups of events with different levels of signal-to-noise ratios of the Moho signal relative to the noise in front of zero delay time (the  $P$  arrival time). Only arrivals with consistent signals were used.

## 4 RESULTS

### 4.1 Crustal structure

Figs 3–5 show stacks of moveout-corrected receiver functions. Strong converted phases within the first 20–30 s delay time are caused by the sedimentary cover (especially in the North German–Polish Basin, beneath the Gräfenberg Array, or the East European Platform), discontinuities in the crystalline upper crust or the Moho and its multiple phases. The quality of the observations of the conversions from the mantle transition zone is influenced by higher order multiples and worse recording conditions in the sedimentary basins, as well as a complicated lithospheric structure beneath the

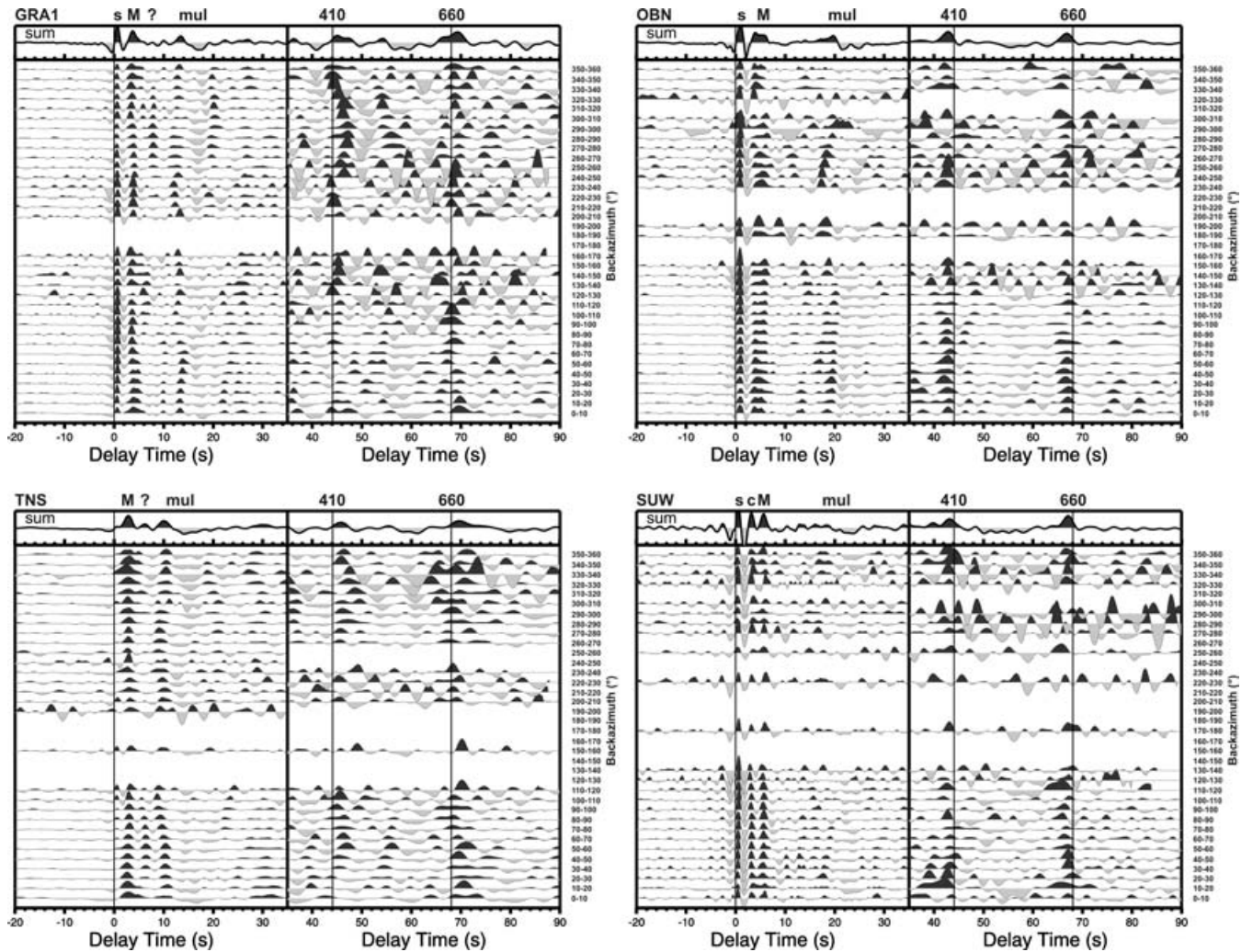


**Figure 3.** Receiver functions stacked in backazimuth windows of  $10^\circ$ . Filters used: high pass  $T_c = 50$ s for time window  $-20$  to  $35$  s; bandpass  $T_c = 3$ s/ $50$ s for time window  $35$ – $90$  s Ps delay time. GRA1. The sedimentary phase (s) and the Moho arrivals (M + mul) are clearly visible over the entire backazimuth range. An additional phase is observed west of the station at about 8 s. The issue of the origin of the phase in the crust (as multiple) or in the mantle (primary phase) cannot be resolved with only one station. Note also the strong and extremely delayed conversions from the 410 km discontinuity west of GRA1, which seem to correlate with the phase at 8 s. The apparent  $P_{410S}$  phase is the strongest 410 km discontinuity observed in central Europe. Unfortunately, to date we have no control on the origin of this phase from other stations. It is possible that there exists a local structure within the uppermost mantle (or even the crust) that causes apparent deepening and focusing of the converted phases from the 410 km discontinuity. OBN. Strong conversions from the sedimentary cover and lower crust can be observed. Moho conversion is assumed at 5.3 s. It is partly masked by the conversion from top of lower crust at 4 s. Conversions from the MTZ clearly arrive before the theoretical arrival times (IASP91). TNS. Again, clear Moho phases can be observed. A questionable phase is visible at about 6–7 s in the northeast. The 410 and 660 km discontinuities are also observable in distinct backazimuth windows. SUW. Strong conversions from the sedimentary cover (and crust) can be observed. Moho conversion is assumed at about 5 s. Conversions from the MTZ clearly arrive before the theoretical arrival times (IASP91).

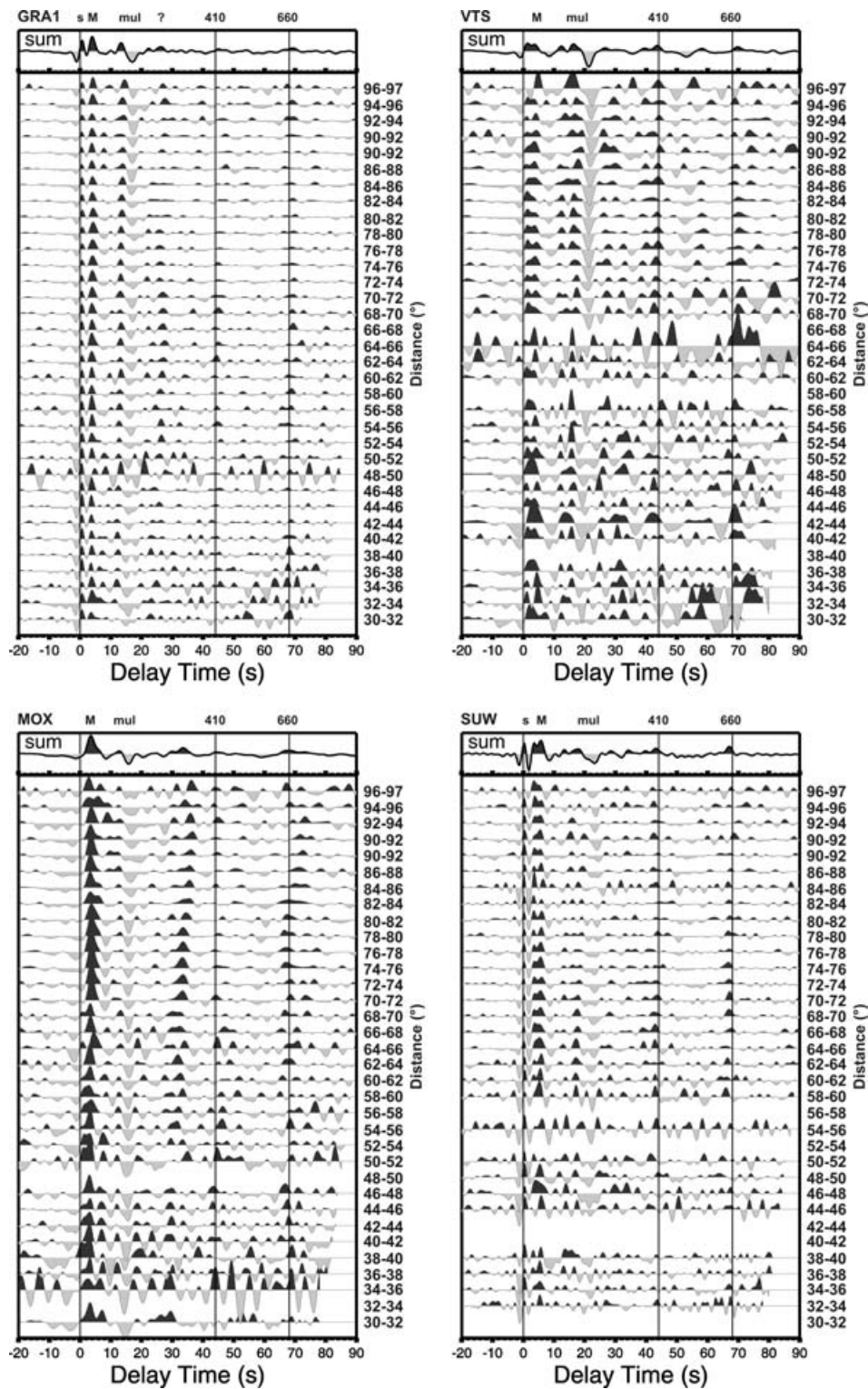


**Figure 4.** Receiver functions stacked in distance windows of  $10^\circ$ . Filter used: bandpass  $T_c = 3\text{s}/50\text{s}$ . GRA1. Primary phases can be attributed to the base of sediments (s) and the Moho (M). Multiples (mul) show clear moveout with distance. Phase marked by “?” probably represents a multiple phase, because additional moveout can be observed. Phases from the 660 km discontinuity show no moveout, whereas the 410 conversions seem to interfere with some multiple energy. However, we think that the 410 can be identified in the stack trace. VTS. Moho, 410, and 660 phases show no additional moveout, which indicates primary conversions. Moho multiples (mul) show remaining moveout. MOX. Moho arrival seems to be more complicated for this station (see also Geissler *et al.* 2005). The first multiple is weak in comparison to the second (negative) multiple. Between 30 and 40 s, a very strong phase can be observed, which shows a large moveout. Assuming horizontal discontinuities, it could be the first multiple of a discontinuity at a depth of about 80 km, or it may represent a second-order multiple from the Moho. There is almost no signal from the 410 whereas the 660 can clearly be seen, also in single stacks. SUW. The Moho, its multiples, the 410 and 660 phases can clearly be identified by their moveout.

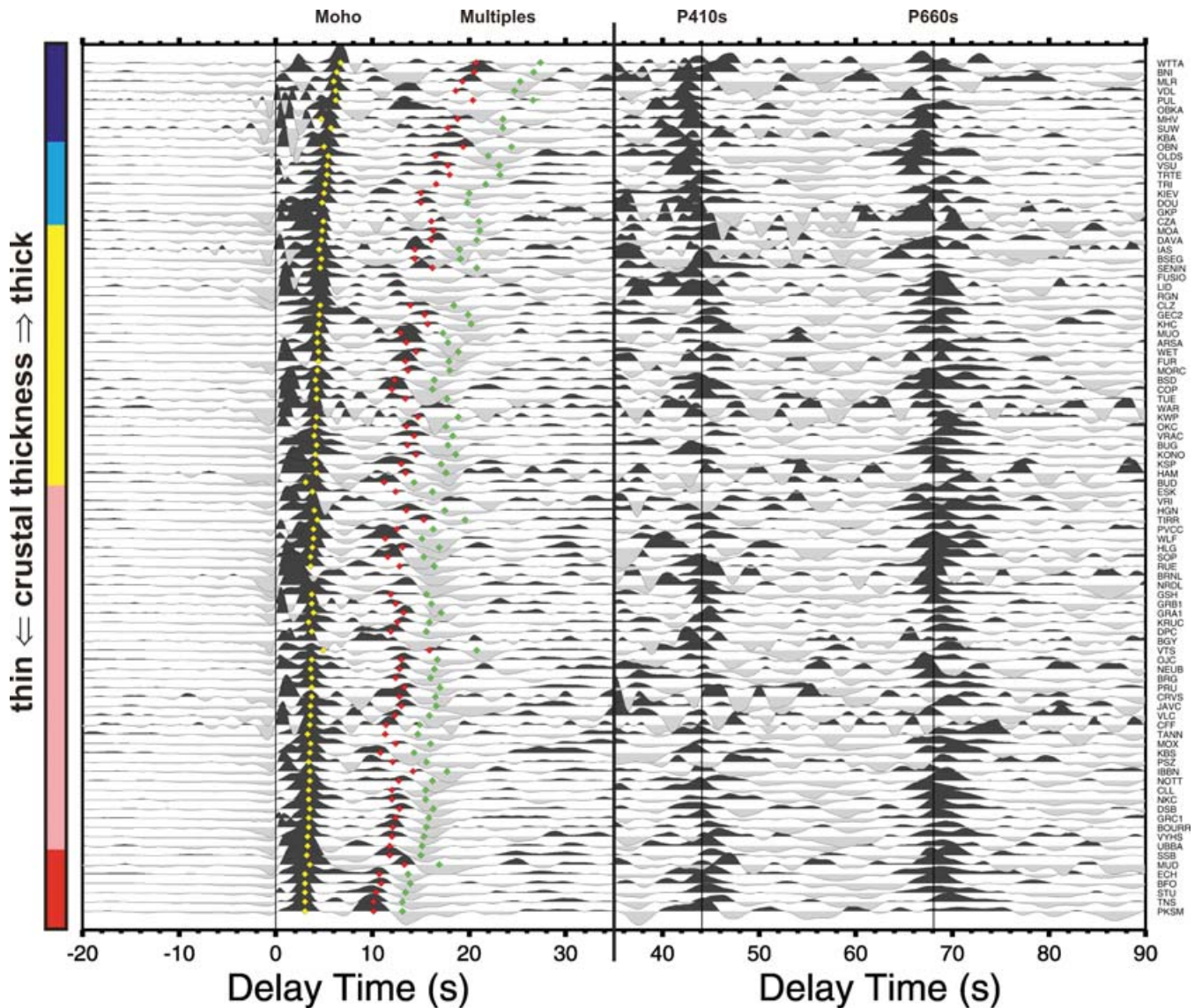


**Figure 5.** Stacked moveout-corrected traces of all stations used. Traces were filtered with a high-pass filter (corner period 50 or 30 s). Theoretical delay times of the 410 and 660 conversions predicted by the IASP91 velocity model (Kennett 1991) are marked by vertical lines. The time window for delay times of from 35 to 90 s was enhanced by a factor of about 3.5 to make the conversions from the mantle transition zone more visible. The calculated delay times of primary and multiple converted phases from the Moho, using the crustal thicknesses and  $V_p/V_s$  ratios from Table 1, are marked.

active orogens. However, the stations on crystalline rocks in consolidated areas show excellent converted phases in most cases.

Generally, the most pronounced phase is the conversion at the Moho, which occurs at a delay time of between <3 and >6 s (Table 1, Figs 5, 6). Amplitudes of the Moho Ps conversions correspond to approximately 10 per cent of the amplitude of the primary P phase (see Table 1). At some stations (e.g. NRDL, BRNL and HAM), the strongest conversion occurs at the base of the sedimentary basin. This masks the converted energy from the crust–mantle boundary. The Moho Ps delay times (Moho depths) agree to a large extent with previous regional receiver function studies as well as with results of regional deep seismic transects. A very shallow Moho (less than 3 s Ps delay time) can be observed in areas under extension, such as the Upper Rhine Graben area (ECH, BFO, STU and TNS) or the Pannonian Basin (PKSM). Late Moho Ps arrivals (up to more than 6 s Ps delay time) can be observed in the Alps (e.g. BNI, WTTA), the

Carpathians (MLR) and the EEC (e.g. SUW, TRTE/VSU and PUL); see Fig. 6. Apart from the direct conversion from the crust–mantle boundary, strong multiples can also be observed, which have been used to analyse Moho depths and crustal  $V_p/V_s$  ratios (Figs 17 and 18) using the approach of Zhu & Kanamori (2000). The uncertainties of the crustal parameters are about  $\pm 0.1$  s for Moho Ps delay time, less than  $\pm 2$  km for crustal thickness and  $\pm 0.05$  for crustal  $V_p/V_s$  ratio (see Geissler *et al.* 2005).

#### 4.2 Mantle transition zone

An approach widely used for studying the depth of the seismic discontinuities in the upper mantle is the common station stacking of the moveout-corrected single traces from all backazimuths. Since the stations analysed are not uniformly distributed within the study area, we used this approach rather than common conversion point

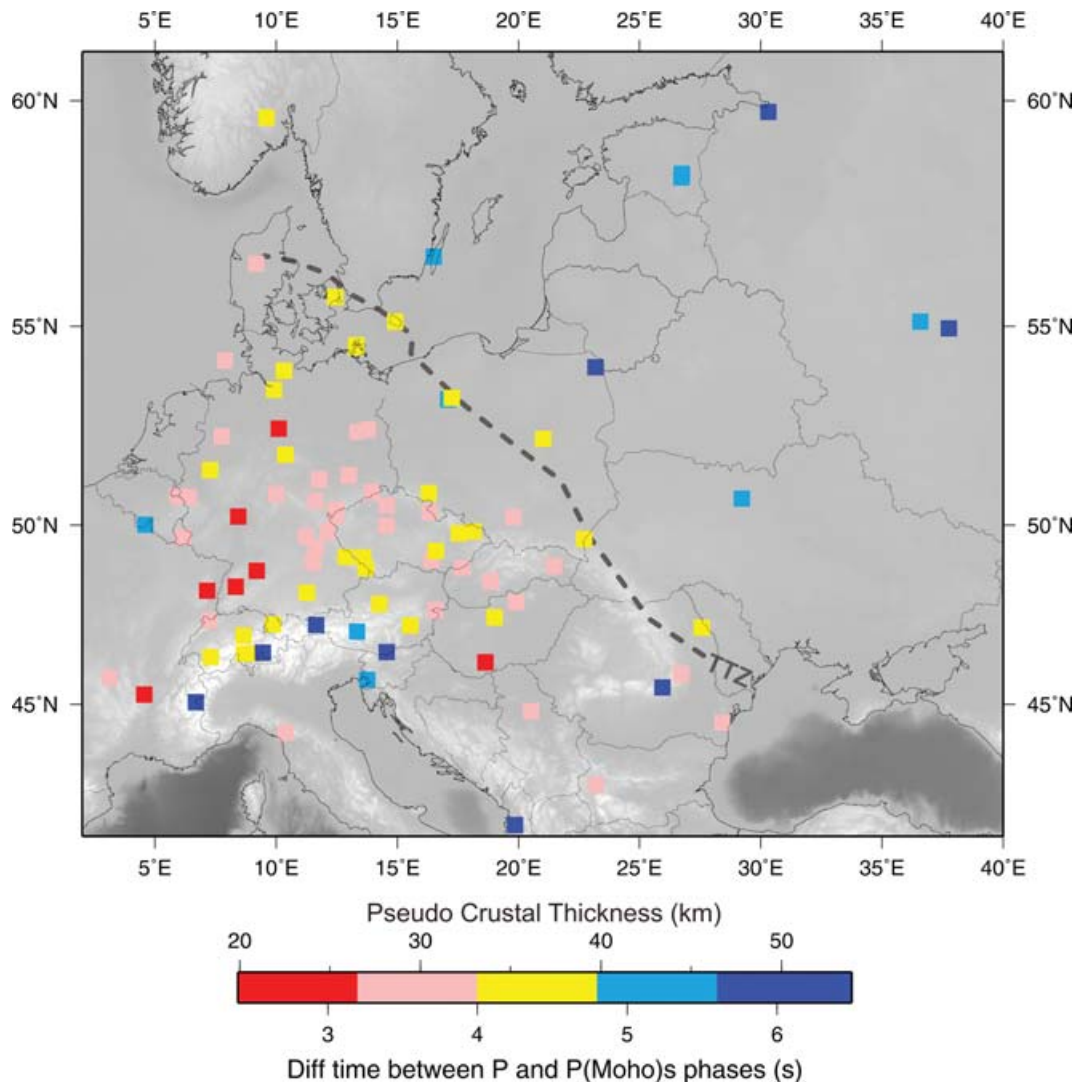


**Figure 6.** Map of Moho Ps delay times and pseudo depths. The delay times were converted to depth using a constant  $V_p/V_s$  ratio of 1.73. Very shallow Moho (red) is indicated beneath the European rift system from the Rhone graben (SSB) to stations close to the Upper Rhine graben (ECH, BFO, STU and TNS). Shallow Moho at NRDL to the north is questionable, because the Moho phase might be masked by crustal reverberations. In addition, PKSM in the Pannonian basin shows an early Moho conversion (shallow Moho). Most stations in central Europe show Moho Ps delay times of  $\sim 3.7$  s (light red;  $\sim 30$  km depth). Stations in old massifs, close to the Alpine orogen, and close to the western border of the East European Craton, show Moho Ps delay times of from 4 to 4.8 s (yellow; 33–40 km). The largest Moho Ps delay times, of up to  $>6$  s, can be observed in the Alps, the Carpathians, and in the EEC northwest of the TTZ (light and dark blue).

stacking, because the latter approach is mainly used for densely spaced temporary networks. The converted phases from the 410 and 660 km discontinuities can be observed at most stations at delay times of about 42–46 and 66–70 s, respectively (Table 1). Their amplitudes are about four times lower than those from the Moho conversions (about 2–4 per cent of the incoming  $P$  wave). Generally, no direct dependence of the delay times of the mantle transition zone on the Moho Ps delay time is observed (see Fig. 5). Delayed arrival times of the 410 and 660 km discontinuities of up to 2 s (in comparison to theoretical delay times calculated from IASP91 Earth reference model) are observed in central Europe, for instance, at stations WLF, TNS, GRA1 and NOTT, as well as at several stations in the western Alps. In contrast, all stations in eastern Europe (on the EEC) show earlier arrivals, both from the 410 and 660 km discontinuities (Figs 9 and 10). The differential travel times for the transition zone ( $P_{660S}-P_{410S}$ ) are about  $23.8 \pm 0.5$  s for most of the stations in central and eastern Europe, as predicted by the IASP91

reference model (Figs 10 and 11). However, in the eastern Alps and the Carpathian–Pannonian region, the MTZ measured by receiver functions seems to be thicker than normal ( $>25$  s differential delay time).

As observed in previous studies (e.g. Kind & Vinnik 1988), the conversion amplitudes and delay times of the 410 km discontinuity may vary with azimuth and frequency. The same is true for the 660 km discontinuity. However, in our stack traces, the 660 km discontinuity is clearer than that of the 410 at most of the stations. The most pronounced conversions from the MTZ can be observed at stations on the EEC.

#### 4.3 Phases around 30 and 54 s Ps delay time

At many stations, additional converted phases can be observed at Ps delay times of around 30 and 54 s (for instance, stations MOX,

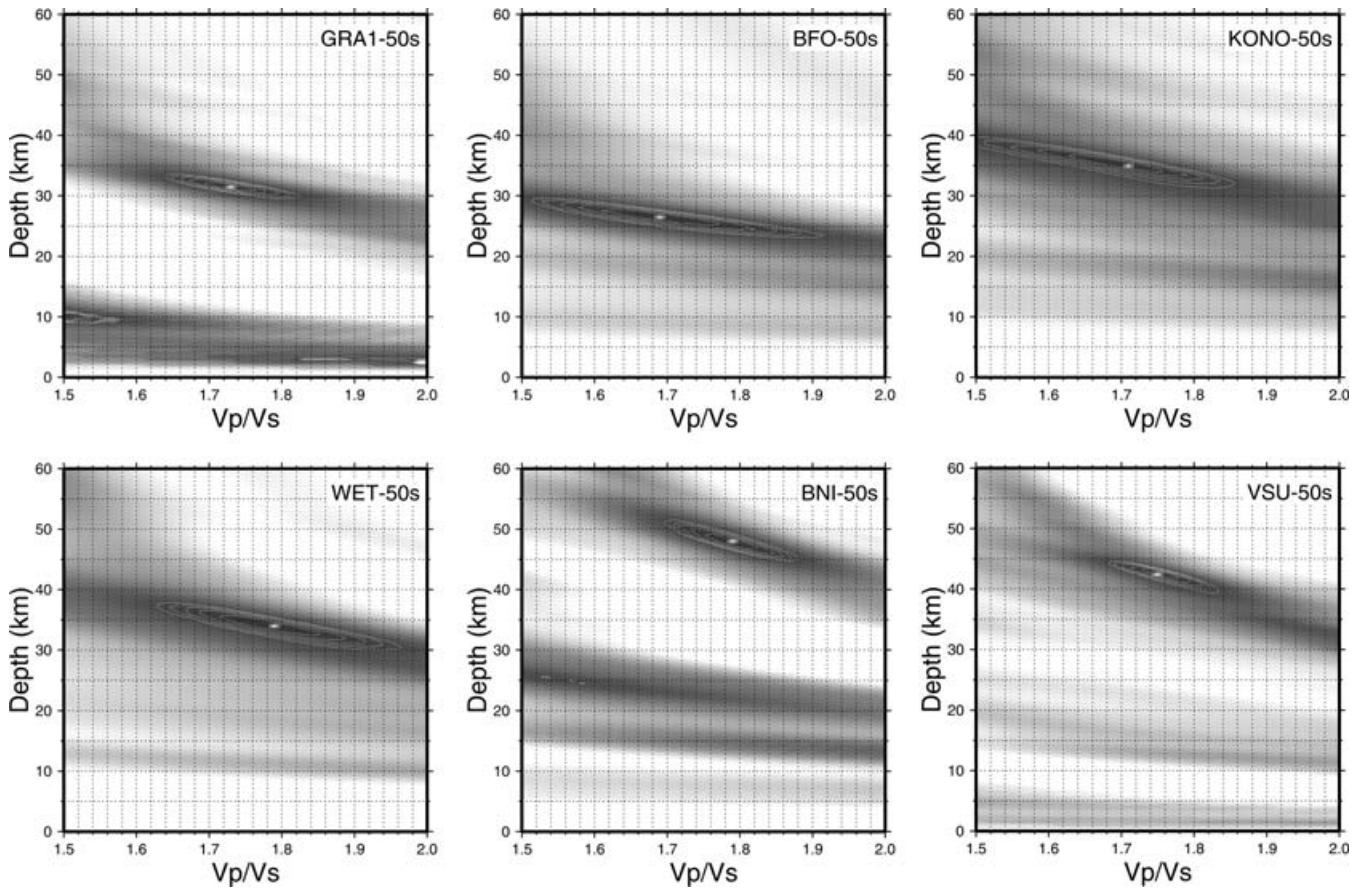


**Figure 7.** Examples of analyses of crustal thickness (Moho depth) and  $V_p/V_s$  ratio after Zhu and Kanamori (2000). Ellipses mark the area with 95–99 per cent of the maximum stacked amplitude, respectively, and can be used as an indication of the uncertainty of the method.

RGN, KWP, MLR, BFO and ARSA). By investigating the distance (slowness) dependence of these phases, we found that in most cases, these phases are multiples of the lithospheric structure; hence, they most probably represent multipath crustal reverberations. This is also indicated by results obtained from analysis of the synthetic receiver functions (next section). These second-order multiples are an indication of a very strong velocity difference at the Moho and minor scattering/damping of the long-period waves within the crust. This agrees with the already very strong ‘primary’ multiples observed at these stations.

#### 4.4 Synthetic receiver functions

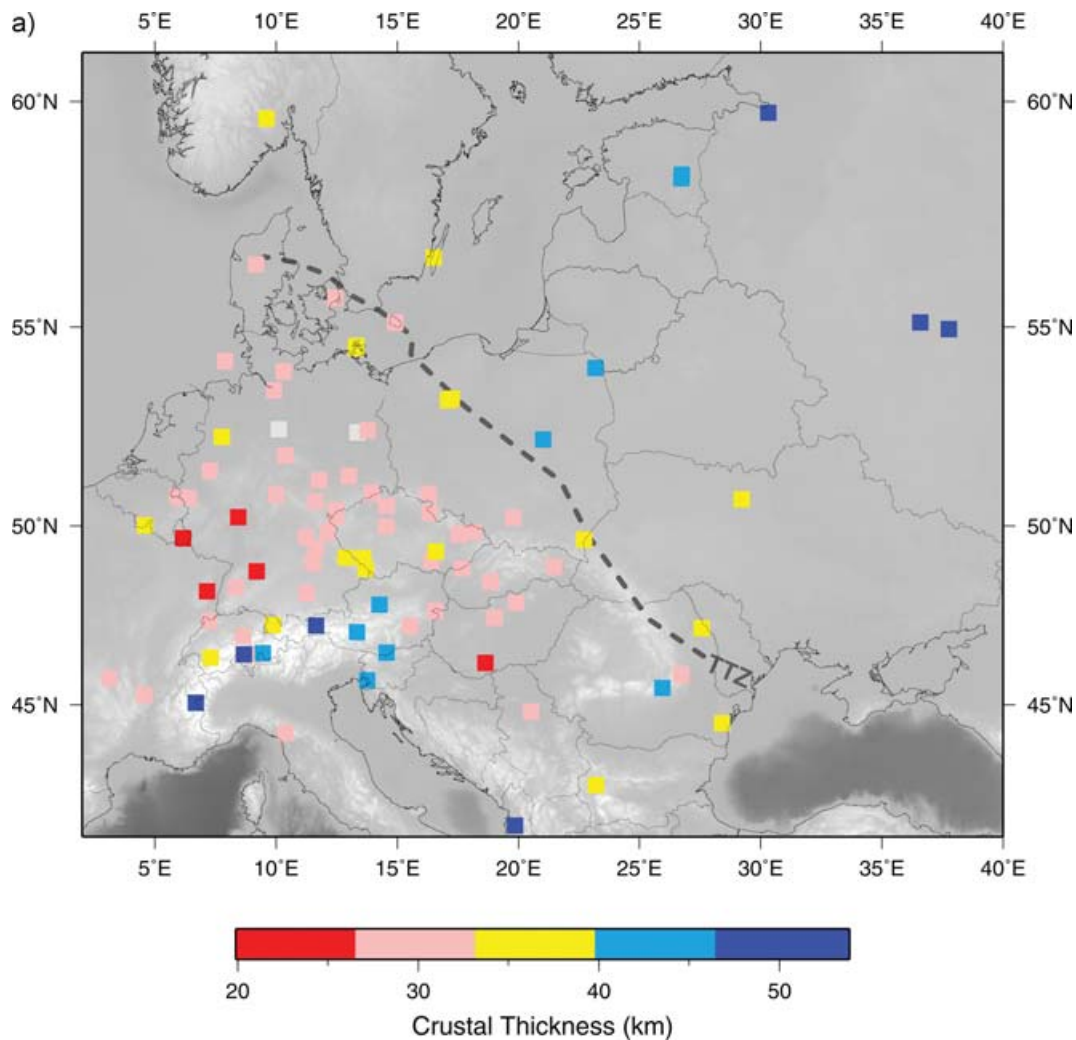
In order to study the cause of the delayed or earlier arrivals from the MTZ converted phases at different stations, we computed receiver functions from synthetic seismograms (Figs 11 and 12) using the reflectivity method (Kind 1985). We used models of seismic velocity that reproduce the differences in crustal structure between central and eastern Europe and tried to vary the seismic velocities in the upper 200 km of the mantle, where significant differences have previously been shown to exist between eastern and central Europe. As can be seen in Fig. 10, the first 20–30 s are dominated by crustal primary conversions and reverberations. It is for the BM3A model (BM; Bohemian Massif), where sharp boundaries of a low velocity zone (LVZ) in the upper-mantle (asthenosphere) exist, that clear conversions can be observed from these discontinuities, at about 9 and 24 s delay time. Smoothing the LVZ boundaries (model BM3B,

Fig. 12) makes the converted phases less significant. In noisy data or at stations with more complicated crustal structure, these phases might not be observable in Ps receiver function data. Clear arrivals can be modelled for both the 410 and 660 km discontinuities. As observed in several tests, the arrival time depends more on the  $V_p/V_s$  ratio than on the absolute velocities in the upper mantle. Model EEC4D (EEC) causes earlier Ps phases from the MTZ, which occur at 42.7 and 66.6 s ( $dt = 23.9$  s). From the IASP91 reference model, we obtained arrival times of 44.2 and 68.0 s ( $dt = 23.8$  s). From models BM3A and BM3B, we obtained values of 45.4/45.1 s and 69.2/68.9 s ( $dt = 23.8/23.8$  s), as summarized in Table 2. Models with lower or higher absolute seismic velocities in the upper mantle but with the same  $V_p/V_s$  ratio as in the IASP91 model show almost no deviation of the MTZ arrival times from the predicted values (BM1A: 44.3/68.1 –  $dt = 23.8$  s; EEC4C: 44.1/67.9 –  $dt = 23.8$  s).

## 5 DISCUSSION

### 5.1 Crustal parameters: Moho depth and $V_p/V_s$ ratio

Crustal thickness in central and eastern Europe has previously been investigated mainly by active seismic studies (both steep and wide-angle), the results of which show that the typical thickness beneath the Palaeozoic platform is about 30 km. This value can reach up to 50 km beneath the EEC, and an even deeper crust–mantle boundary has been observed beneath parts of the Alpine–Carpathian orogenic belt (e.g. Giese 1995; Grad *et al.* 2002; Dezes *et al.* 2004).



**Figure 8.** (a) Map of crustal thickness and (b) crustal  $V_p/V_s$  ratios as estimated by the method of Zhu & Kanamori (2000). Grey squares mark stations where no reliable estimates could be achieved.

The Moho depths obtained in this study (Table 1, Fig. 8a) agree very well with previous results obtained from active-source studies and reflect the location of stations within different tectonic provinces (Pre-Cambrian craton, Palaeozoic massifs and Cenozoic areas under extension or compression). In addition, the Moho pseudo depths obtained from Ps delay times agree quite well with the Moho depths obtained by the Zhu and Kanamori method (compare Figs 6 and 8a). However, no clear dependence of the calculated  $V_p/V_s$  ratio on the major tectonic regime exists. Even if  $V_p/V_s$  ratios do not exhibit differences between the major tectonic units, there seem to be consistent areas within these units that show similar  $V_p/V_s$  ratios. Increased  $V_p/V_s$  ratios can be observed at stations in northern Germany, southern Sweden/eastern Denmark, in the Sudeten mountains at the Czech–Polish border and at stations in the Alpine–Carpathian orogenic belt. Stations with a lower than average  $V_p/V_s$  ratio (red in Fig. 8b) are more scattered, showing no consistent spatial distribution. Some stations show anomalous low or high  $V_p/V_s$  ratios, which might not be realistic. This might then also apply for the corresponding Moho depth values. It is probable that the very complicated low values observed are caused by complicated crustal structure (wave paths, for example, caused by a high-velocity lower crustal layer, as may be the case for stations MHV and OBN) and therefore, inter-

ference of intracrustal multiples with direct Moho conversions or Moho topography, as discussed by Geissler *et al.* (2005) and Zandt *et al.* (1995). From our data we conclude that the  $V_p/V_s$  ratio depends more on local crustal structure and composition than on the age of the tectonic unit.

## 5.2 Upper mantle: apparent topography and depths of the 410 and 660

Previous studies of the seismic discontinuities of the mantle transition zone beneath central Europe were carried out with data from permanent stations (Kind & Vinnik 1988; Stammer *et al.* 1992; Grunewald *et al.* 2001) as well as from temporary experiments (e.g. TOR & SVEKALAPKO – Alinaghi *et al.* 2003; EIFELPLUME – Budweg *et al.* 2006). Grunewald *et al.* (2001) investigated the topography of these discontinuities in Germany using data from the German Regional Seismic Network (GRSN) and the Gräfenberg Array (GRF). We extend this work by including more data from German stations and adding data from other permanent broad-band stations in central and eastern Europe (Fig. 2).

As mentioned above, apart from the Moho depths, the most striking difference between eastern and central Europe can be observed

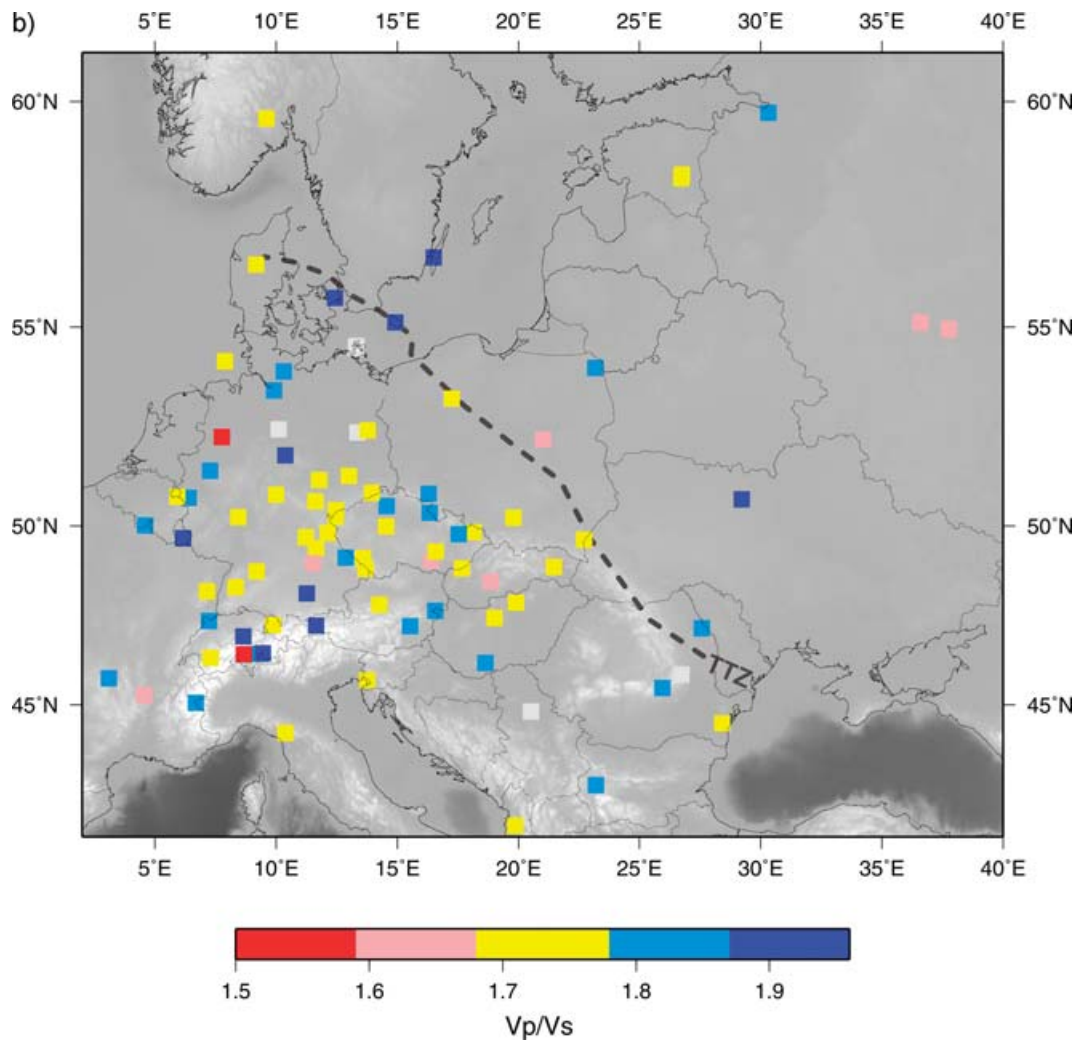


Figure 8. (Continued.)

in the absolute  $P_s$  delay times of the mantle transition zone discontinuities. In eastern Europe, they arrive up to 2 s earlier than predicted by the IASP91 Earth reference model, whereas in central Europe they show a delay of up to 2 s (Figs 10a and b).

Although there appears to be sufficient data available to study the MTZ in the Alpine–Carpathian region, its complicated lithospheric structure hampers easy identification of the converted phases from the MTZ. At some stations, multiple phases seem to mask the MTZ conversions. However, conversions from the 660 km discontinuity can be identified clearly at most stations. These are delayed by up to 2 s in the eastern Alps/Carpathian region, whereas the  $P_{410s}$  conversions identified do not show such dramatic delays. This results in an MTZ that is approximately 20 km thicker (up to 2 s differential delay time) beneath the Carpathian–Pannonian region (e.g. PKSM, VTS, VYHS and KWP) compared to that found in central and eastern Europe.

Fig. 13(b) shows the differential delay time plotted against the  $P_{410s}$  delay time. The dashed line shows the expected correlation by Clapeyron slopes of  $+3 \text{ MPa K}^{-1}$  for the 410 and  $-2 \text{ MPa K}^{-1}$  for the 660 km discontinuity (see Li *et al.* 2003b). An increase in the 410 time for a constant differential time (the area to the right-hand side of the dashed line) can be explained by a decrease in the upper-mantle velocities, which is in most cases accompanied by an increase in the

$V_p/V_s$  ratio in the upper mantle. The converse is true for the area to the left-hand side of the dashed line. It is clear that stations on the EEC are clustered in a small area to the left-hand side of the expected line of correlation. Data from stations in central Europe (Palaeozoic) show a greater degree of scatter and almost all fall to the right-hand side of the correlation line in the plot. This could indicate higher  $V_p/V_s$  ratios on the travel path, because differences in delay times seem to depend to a large extent on the  $V_p/V_s$  ratio of the mantle and crust rather than on the absolute velocities as discussed previously. The general trend in the diagram (plotting along  $t_{\text{diff}} = 24 \text{ s}$ ) confirms results from the global study of Chevrot *et al.* (1999) and indicate that delays in the  $P_{410s}$  (and  $P_{660s}$ ) are caused mainly by the velocity ( $V_p/V_s$ ) structure in the upper mantle.

Significant variations exist between delay times of the 410 km (and 660 km) discontinuity recorded at different stations only some tens of kilometres apart, as for example in the case of the western Bohemian Massif (e.g. stations GRA1, GRB1, GRC1 and NOTT). We therefore, conclude that the main cause of the apparent topography of the 410 km discontinuity might be located in the uppermost mantle very close to the individual stations. Although data from stations in the Alpine–Carpathian belt are more complicated, it may be seen that some stations are plotted at differential delay times  $> 25 \text{ s}$ .

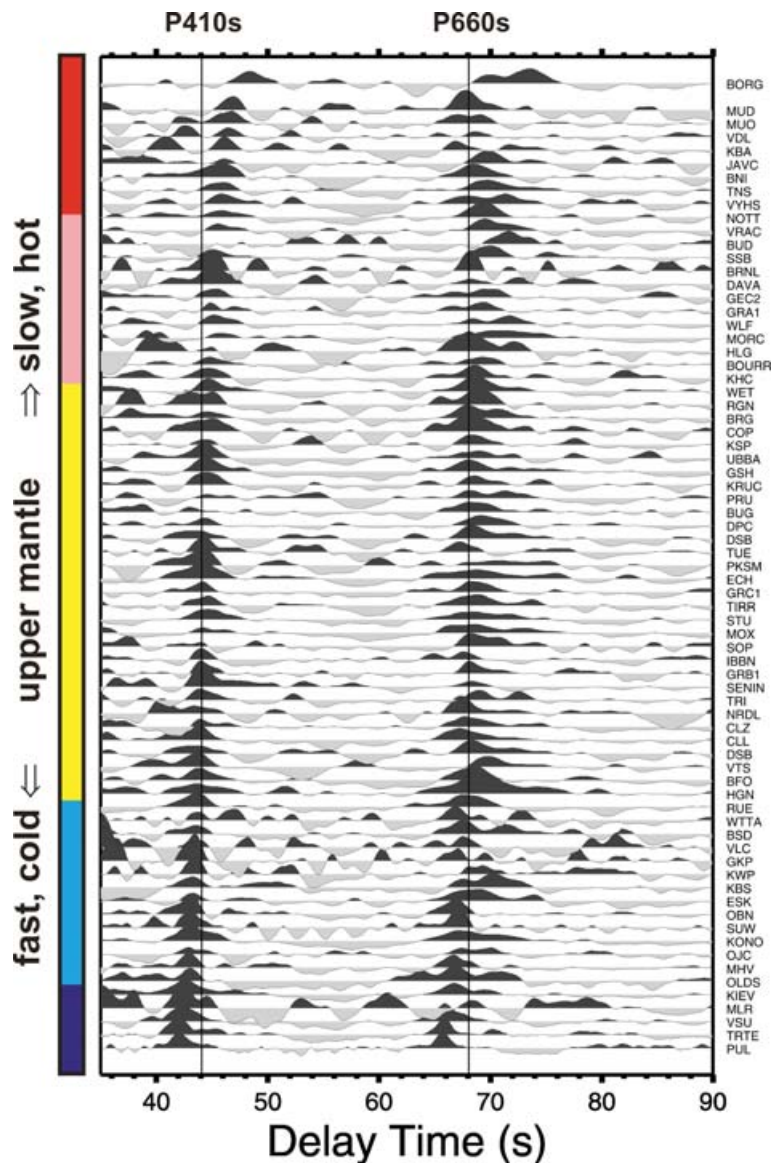


**Figure 9.** Ps converted phases of the mantle transition zone aligned after the arrival time of the conversion from the 410 km discontinuity. Most stations on the EEC show early arrivals for the 410 and 600 km discontinuities, whereas various stations situated in the Alps (BNI, MOA), close to active volcanic areas or graben systems (MUD, NOTT, TNS and WLF) or on top of sedimentary basins show late arrivals for the 410 km discontinuity. Assuming that the delay time of the 410 km discontinuity would only depend on the average upper mantle velocity structure, this would indicate significant differences in the upper mantle between the EEC and central Europe. Only stations with identified arrivals of 410 km discontinuities are shown.

### 5.3 Mantle transition zone: thickened MTZ beneath SE Europe

As stated above, we observed significant variations in transition zone thickness across central and eastern Europe. Beneath central Europe north of the Alps and the EEC, the transition zone thickness is close to the value found in the IASP91 global reference model. Beneath the eastern Alps, the Pannonian Basin and the Carpathians, the transition zone seems to be more than 20 km (up to 2 s differential delay time) thicker than the IASP91 reference value, whereas beneath the western Alps, the extent of the thinning and thickening appears to be mixed. According to Bina & Helffrich (1994), variations in thickness of  $\pm 20$  km could be explained as variations in temperature of  $\pm 150$ –200 K within the MTZ. This would imply at least a 150 K cooler mantle transition zone beneath

the Carpathian–Pannonian region. The slightly reduced differential delay times (compared to the IASP91 model) of more than 1 s less at stations BNI, TUE, VDL and MUO in the western Alps would translate into an approximately 75 K hotter MTZ in that area. North of the Alpine–Carpathian belt, the temperature variations seem to be negligible. In particular, there seems to be no difference between the temperatures of the mantle transition zone beneath the Variscan consolidated central European platform and the Pre-Cambrian EEC. If these estimates of temperature variation are correct, this results in lateral temperature variations in the mantle transition zone beneath central and eastern Europe of about 225 K.

The observed thickening of the MTZ beneath the eastern Alps and the Carpathians may be explained by the model of, for example, Piromallo *et al.* (2001) and Piromallo & Facenna (2004), who postulate old subducted (cold) slabs in the MTZ beneath large parts

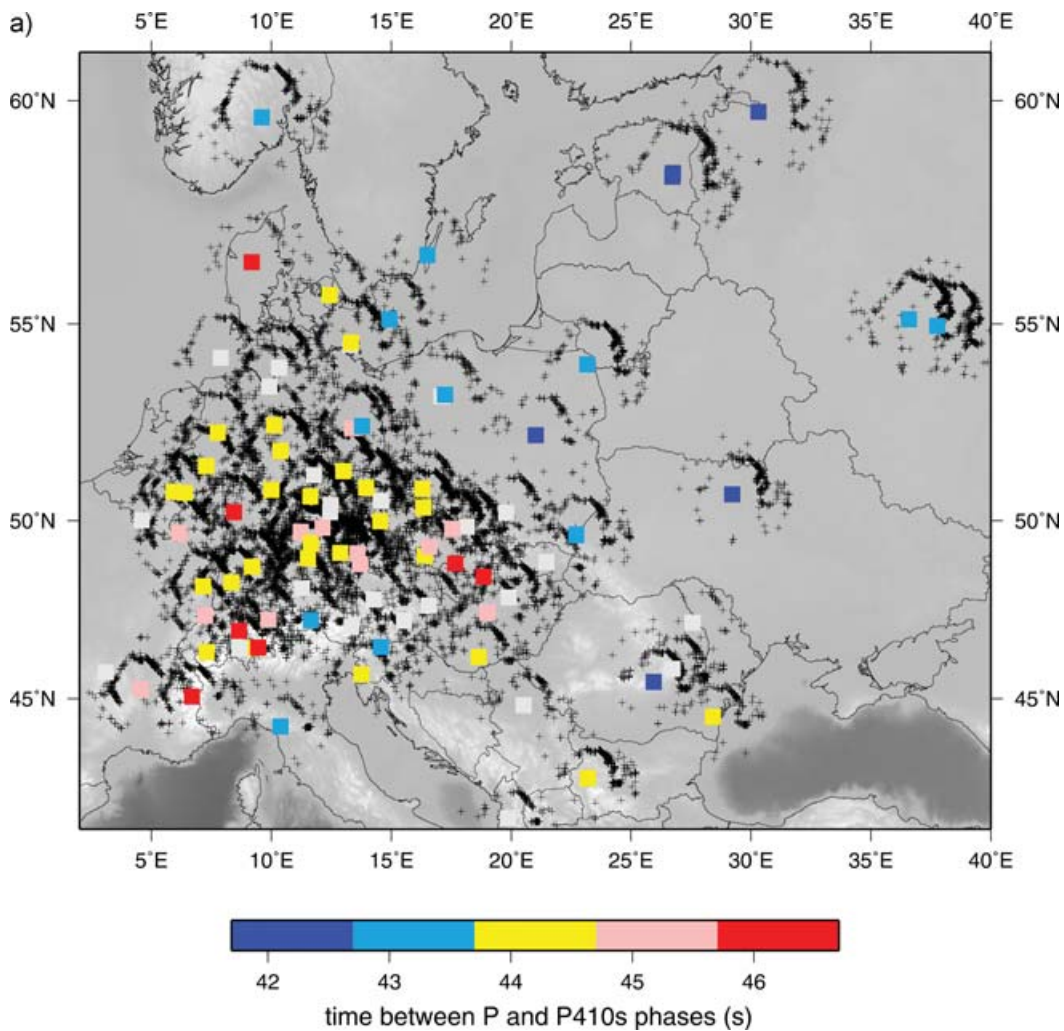


**Figure 10.** (a) Ps delay times for converted phases from the 410. Red colours indicate apparent deepening (later arrivals), blue colours apparent shallowing of the 410. Almost all picks for central Europe are in the range  $44.2 \pm 0.5$  s delay time (yellow squares), whereas earlier arrivals are observed at stations on the EEC (blue). The situation beneath the Alpine belt is inhomogeneous. It is obvious that at some localities within a small area, we observe very different delay times (see also Fig. 5). Grey squares mark stations where no clear identification of the  $P_{410s}$  could be made. (b) Ps delay times for converted phases from the 660. Most stations in central Europe show arrival times close to the IASP91 value of  $68.0 \pm 0.5$  s (yellow). Stations on the EEC show early arrivals (blue), whereas stations in the eastern Alps and Carpathian area show very late  $P_{660s}$  arrivals (red). Grey squares mark stations where no clear identification of the  $P_{660s}$  could be made. (c) Differential Ps delay times for converted phases from the 410 and 660. Red colours indicate smaller differential Ps delay times than indicated by the IASP91 velocity model (thin transition zone). Blue colours indicate larger values. Most of central and eastern Europe shows values close to the IASP91 value of  $23.8 \pm 0.5$  s. Stations at the western rim of the western Alps show slightly enlarged differential delay times, whereas stations within the western Alps show smaller values. Strongly enlarged values are indicated beneath the eastern Alps and the Carpathian belt (See also Fig. 13). Grey squares mark stations where no clear identification of the MTZ conversions could be made.

of southeastern Europe. The strongest indication for thick accumulated cold material (former oceanic slabs) can be found in the area marked by Piromallo & Facenna (2004; Fig. 1) with ‘Carpathian’. In this region, very high  $P$ -wave velocities are mapped at depths of 650 km. The authors also find similarly high velocities beneath the (western) ‘Alps’, where we observe enlarged differential delay times only at stations at the western rim, with stations within the western Alps showing reduced values. This could point to a more complicated structure of the mantle transition zone in this area than previously described. The thickening of the MTZ beneath the eastern Alps, the Carpathians and the Pannonian Basin is comparable to SW Japan, where a thickening of the MTZ of about 30 km was observed by Tonegawa *et al.* (2006). It may well be the case that a large flat (cold) slab rests within the mantle transition zone, showing high seismic velocities and causing a thickening of the MTZ. Sur-

prisingly, such a thickening seems not to exist beneath Tibet, where the thickness of the mantle transition zone is close to the IASP91 values (Yuan *et al.* 1997; Kind *et al.* 2002). It may be assumed that in the case of SW Japan and southeastern Europe, the subduction processes reach into the mantle transition zone, whereas in Tibet, processes related to continental collision seem to stop above the 410 km discontinuity.

According to Swieczak *et al.* (2004), the thickness of the mantle transition zone beneath eastern Europe varies from 240 to 280 km. Swieczak *et al.* assumed a thicker MTZ beneath the Pre-Cambrian platform (cold lithosphere), whereas the MTZ should be thinner beneath the Carpathians (hot lithosphere). Our results do not confirm the assumptions regarding the MTZ thickness made by Swieczak *et al.* (2004). They agree more with results from North America instead, which also fail to show any imprint of the cold lithosphere

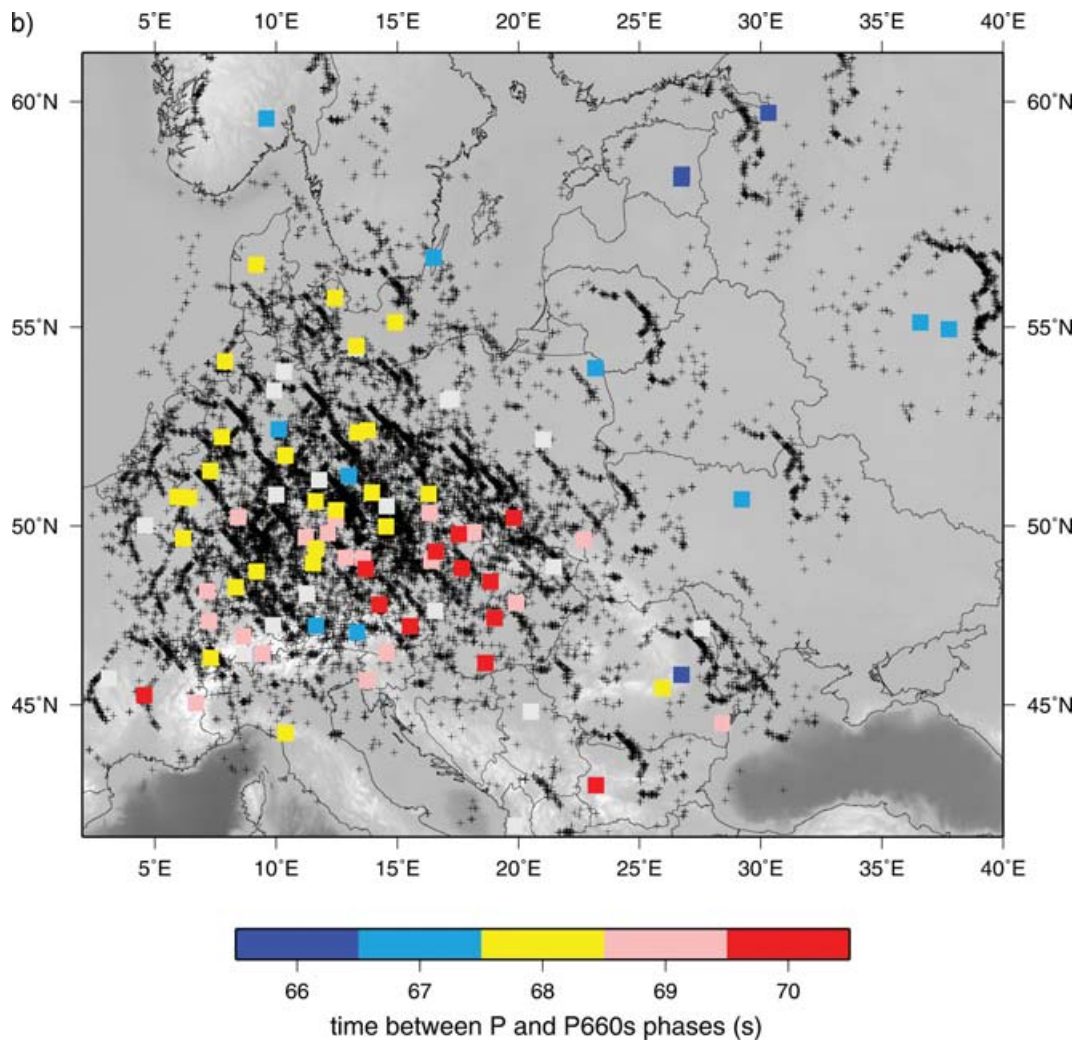


Figure 10. (Continued.)

of the continental keel on the mantle transition zone thickness (Li *et al.* 1998) and thus indicate a decoupling of the EEC lithosphere (tectosphere) from the MTZ. Ramesh *et al.* (2002) observed a depression of the 410 km discontinuity by about 2 s in the western USA, which confirms a seismically slow upper mantle and probably has no imprint on the MTZ.

Apparent local deepening of MTZ discontinuities is also indicated in our results for specific backazimuth windows at single stations. We observe an apparent deepening of the 410 km discontinuity northwest of GRA1 (Fig. 3), as well as a local deepening of the 660 km discontinuity northeast of BFO. However, the data is presently too sparse (caused by the stations being too far apart) to analyse these structures in more detail. The observed anomalies may well be related to small-scale depth variations of the MTZ discontinuities close to the Eifel Plume (Budweg *et al.* 2006), but could also be caused by complex upper-mantle structures.

#### 5.4 Influence of non-olivine component phase transformations

The preceding discussion was based on the assumption that all the seismic discontinuities of the mantle transition zone are domi-

nated by the transformations of the olivine component. However, as shown by different authors (e.g. Revenaugh & Jordan 1991; Vacher *et al.* 1998; Deuss *et al.* 2006), the transformations of garnet-to-ilmenite and ilmenite-to-perovskite may also have an effect on the seismic velocity distribution, depending strongly on the temperature regime. As shown by Vacher *et al.* (1998), ilmenite is stable in cold regions (1000 K adiabat). Multiple phase transitions should, therefore, occur at depths of from 620 to 710 km, especially in garnet or MORB rich material, in a manner similar to some subducted oceanic slabs. According to Vacher *et al.* (1998), the gt-sp breakdown occurs in a very sharp (pressure/depth) interval (*ca.* 2 km thickness). The ilmenite transitions (gt-ilm, ilm-pv) are about 22 and 56 km thick, respectively, and may, therefore, be invisible in high-frequency seismic data. In hotter regimes, most of the seismic gradient is caused by the ‘olivine’ transitions; only a small gradient below the 660 km discontinuity might be the contribution from the ‘garnet’ transitions.

Using high-pressure mineralogy and physics, it can be shown that there appear to exist multiple transitions, especially at the base of the mantle transition zone. Unfortunately, the seismic data presented so far is unconvincing. Simmons & Gurrola (2000) and Niu & Kawakatsu (1996), for example, showed indications for multiple seismic discontinuities, although they did not show that the observed

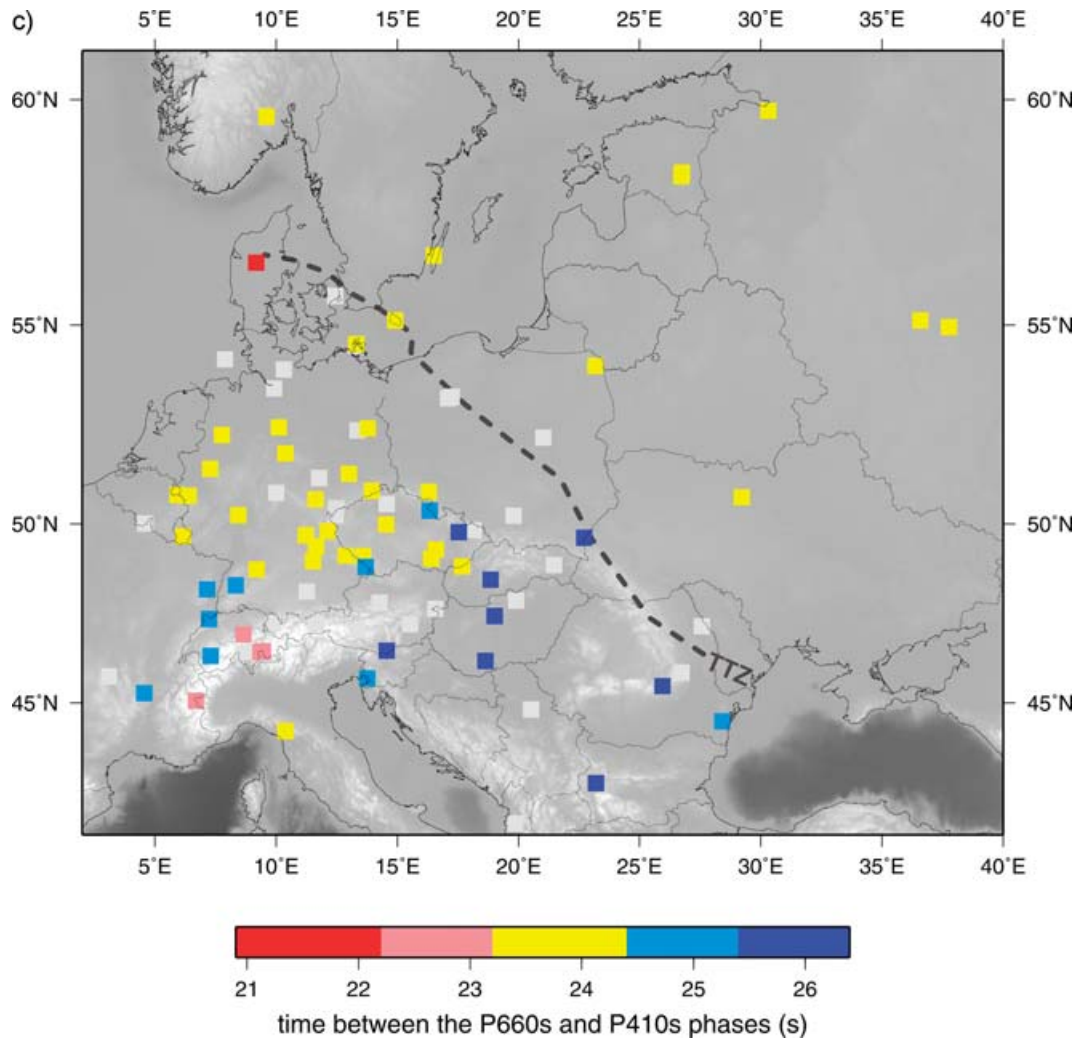


Figure 10. (Continued.)

**Table 2.** Delay times of the 410 and 660 km discontinuities obtained from the synthetic receiver functions (Figs 11 and 12). For model parameters, see Table A2.

Model	$t_{ps}(\text{Moho})$ (s)	$t_{P410S}$ (s)	$t_{P660S}$ (s)	$dt_{660-410}$ (s)	$n$
IASP91	4.6	44.2	68.0	23.8	27
BM1A	3.8	44.3	68.1	23.8	27
BM3A	3.8	45.4	69.2	23.8	27
BM3B	3.8	45.1	68.9	23.8	26
EEC4C	5.9	44.1	67.9	23.8	25
EEC4D	5.9	42.7	66.6	23.9	25

phases are in fact primary conversions. Moreover, Tonegawa *et al.* (2006) did not show any complexity of the 660 conversion in their study in an area close to that of Niu & Kawakatsu (1996). Our own observations of very late (complex and even doubled) phases with delay times of from 68 to 71 s, especially for stations in the eastern Alps and the Carpathians, may of course be related to these multiple phase transitions of the olivine and garnet (ilm-pv) components. In both cases, the late arrivals of the  $P_{660S}$  point to a cold and, therefore, thickened transition zone in that region.

### 5.5 Sharpness of MTZ discontinuities

As previously mentioned, we also observed strong variations in the amplitudes of converted phases from the 410 km discontinuity beneath central Europe. As indicated in our study, the 410 phase might interfere with multipath reverberations from the crust and uppermost mantle at some stations (see Figs 4 and 11). Other possible causes of weak or complicated  $P_{410S}$  phases are strong topography (van der Lee *et al.* 1994) or a broad transition layer (50 km wide) instead of the sharp discontinuity, as discussed by Chevrot *et al.* (1999). Broadening and frequency dependence of the  $P_{410S}$  phase could be caused by the presence of water (Wood 1995; Helffrich & Wood 1996; van der Mejde *et al.* 2003). This may cause a '410 transition' up to 40 km wide (Smyth & Frost 2002), in which case a conversion from the 410 km discontinuity would be barely detectable. Furthermore, broadening may occur due to temperature decrease (Bina & Helffrich 1994), which would contradict our observations beneath the EEC where we observed a particularly sharp 410 km discontinuity in all cases, in contrast to stations in central Europe. It is clear that the conversions from the MTZ at stations in the EEC are sharper than at stations in the rest of the study area. We may speculate that beneath the EEC, the discontinuities in the mantle transition zone are also sharper or at least show less small-scale

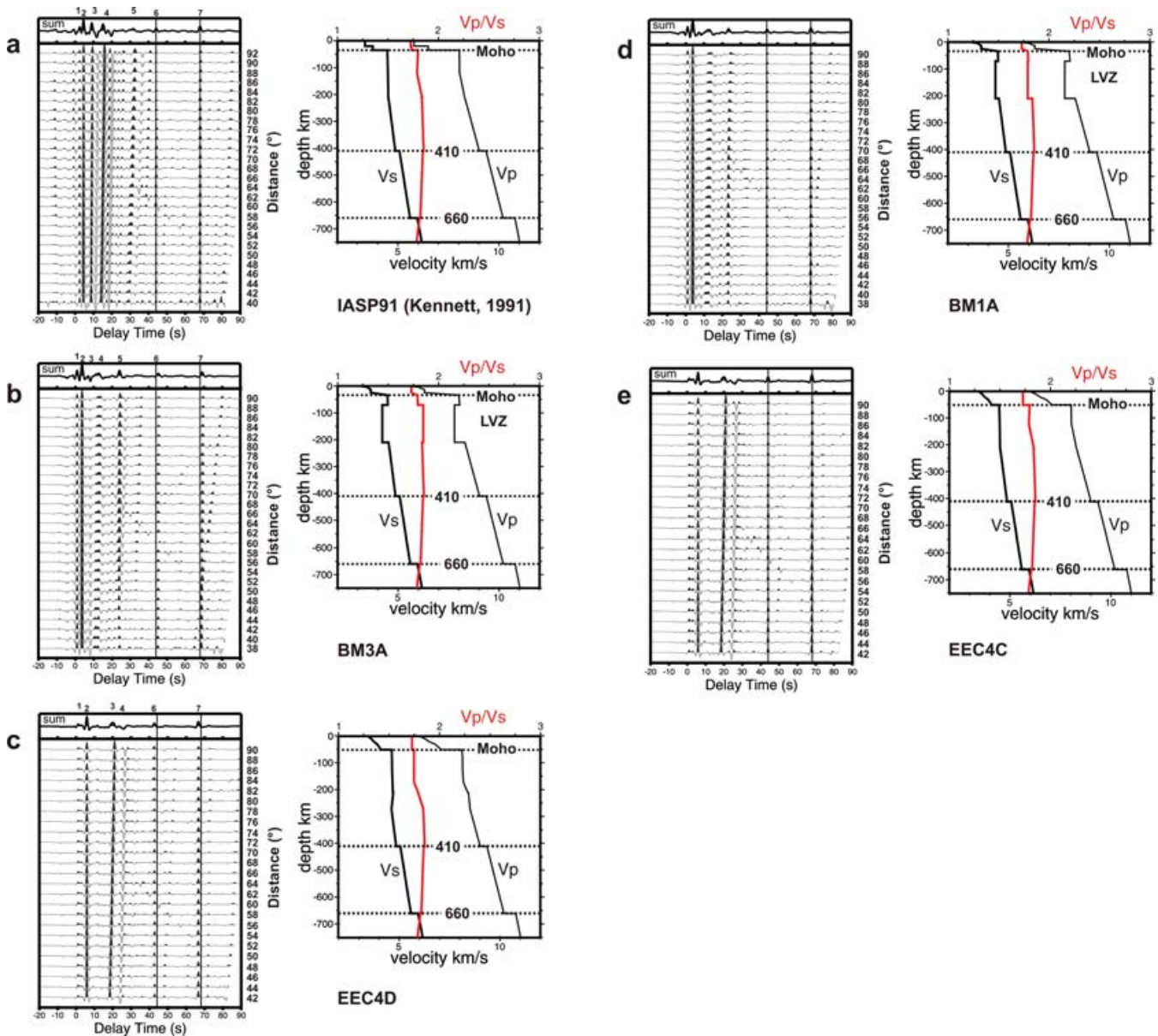


**Figure 11.** Synthetic receiver functions processed from data computed by the reflectivity method. Different crustal and upper mantle models were used for central Europe (b – BM3A, d – BM1A) and the EEC (c – EEC4D, e – EEC4C). The main differences from the IASP91 Earth reference model (a) are an upper mantle low velocity zone (LVZ) in the BM (western Bohemian massif) models and higher upper mantle (shear wave) velocities in the EEC model.

topography. It may also be the case that less damping/scattering of higher frequencies of the converted phases in the upper mantle may be affecting our observations. If Bina & Helffrich (1994) are correct, then the MTZ below the EEC should not be colder than one might expect from the cool thick lithosphere above. In contrast, partly weak 410 conversions in the Carpathian region may be caused by lower temperatures.

### 5.6 Compositional differences in the upper mantle beneath central and eastern Europe

As shown by our synthetic seismogram analysis, most of the apparent deepening/up-warping of the 410 and 660 km discontinuities can be explained by reduced/enlarged seismic velocities/heterogeneity in the crust and uppermost mantle, which was already proposed by

Kind & Vinnik (1988). High  $V_p/V_s$  ratios modelled in the upper mantle (71–210 km depth) of central Europe (models BM3A/B: 1.85; IASP91: 1.80) may be caused by lower seismic  $S$  (and  $P$ ) velocities due to higher temperatures and the presence of small amounts of melt or water (asthenosphere). Different chemical composition cannot alone explain such high  $V_p/V_s$  ratios (Goes *et al.* 2000; Hacker & Abers 2004). Another possible source of high  $V_p/V_s$  ratios ( $>1.8$ ) may be anisotropy, as stated by Kobussen *et al.* (2006). However, if we stack our data over all backazimuths, the effect of anisotropy should be less important (at least at stations with good data coverage).

$V_p/V_s$  ratios as low as 1.75 were modelled for the EEC upper mantle down to 271 km (model EEC4D). Such low values can be partially explained by a cold olivine-orthopyroxene-rich mantle, according to our calculations, using the Excel worksheet of Hacker & Abers (2004). The lower  $V_p/V_s$  ratio might be caused mainly by

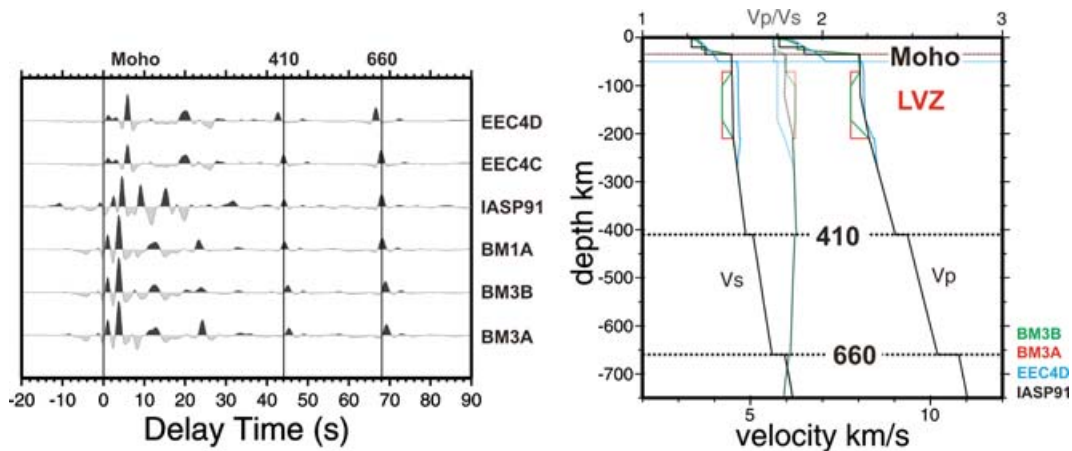


**Figure 12.** Stacked synthetic receiver functions for different models. In addition to the differences in the crustal phases, changing mantle  $V_p/V_s$  ratio significantly influences the arrival times of the MTZ conversion phases, as shown in models BM3A or EEC4D.

higher shear wave velocities (3.5 per cent above IASP91 velocities), which were previously found by surface wave studies (e.g. Zielhuis & Nolet 1994; Cotte *et al.* 2002). According to Kopylova *et al.* (2004), the depleted cratonic mantle is characterized by lower  $V_p$  and higher  $V_s$  (leading to a lower  $V_p/V_s$  ratio) due to opx-enrichment (effect of up to  $0.05 \text{ km s}^{-1}$  for the Slave craton). Kopylova *et al.* (2004) state that many xenoliths from Archean cratons are characterized by extreme depletion, abundant opx and low ol/opx ratios. Xenoliths from the Baltic (Fennoscandian) Shield (Kukkonen & Peltonen 1999) are dominated by harzburgites (up to 77 per cent opx, 'mean': 26 per cent). A xenolith geotherm indicates a temperature of about  $1300 \text{ }^\circ\text{C}$  at a depth of approximately 220 km. High Mg# harzburgites are characterized by lower densities, which support the study by Artemieva (2003), which showed that the upper mantle beneath the NE Baltic Shield is up to 1.4 per cent less dense than typical Phanerozoic mantle. As previously discussed by Priestley & McKenzie (2006), low temperatures should have a greater impact on the shear wave velocities than any variations in chemical composition.

A  $V_p/V_s$  ratio of 1.75 is likely to be the lower limit of what can be explained by isotropic velocities from chemical composition. It is possible that some amount of the observed  $V_p/V_s$  anomalies could also be explained by anisotropic effects, but we cannot explore such a possibility in this study. An opx-rich mantle could explain low  $V_p/V_s$ , but not high  $V_p$  velocities just beneath the Moho as observed in wide-angle seismic studies (e.g. Grad *et al.* 2002). It may be that the observed high  $P$ -wave velocities occur only within a thin layer just beneath the Moho.

## 6 CONCLUSIONS

This receiver-function study confirms previous estimates of crustal parameters in central and eastern Europe. There exist big differences in crustal thickness between Palaeozoic Europe, the EEC and the Alpine–Carpathian belt. Small differences exist between extended and non-extended regions in the Palaeozoic crust. Moho Ps delay times for stations on the Palaeozoic platform are generally  $<4 \text{ s}$  ( $<33 \text{ km}$ ), but can reach more than  $6 \text{ s}$  ( $50 \rightarrow 55 \text{ km}$ ) in the EEC and beneath the Alps/Carpathians. The amplitudes of the converted phases are normally about 10 per cent of the incoming  $P$ -wave amplitude and in the EEC they are generally below 10 per cent. Average crustal  $V_p/V_s$  ratios show no correlation with tectonic age of the station basement. The mean value is 1.76, but the  $V_p/V_s$  ratio varies

from about 1.6 to almost 2.0. However, the accuracy of extreme values is questionable.

The apparent topography of the 410 km discontinuity seems to depend mainly on the  $V_p/V_s$  ratio in the upper mantle (above the MTZ), so the delay of 410 conversions compared to those predicted in IASP91 could be caused mainly by a reduction in shear-wave velocity ( $V_p/V_s$  increase) within the asthenosphere, whereas the early arrivals from the 410 km (and in consequence also partly of the 660 km) discontinuity beneath the cratonic area are caused mainly by higher shear wave velocities, as is also indicated by studies on surface waves (e.g. Zielhuis & Nolet 1994; Cotte *et al.* 2002). High shear wave velocities beneath the craton could be explained by the absence of an asthenospheric layer, low temperatures, and a depleted chemical (opx-rich) composition. Goes *et al.* (2000) interpreted velocity variations in tomography models of Europe at a depth of 80 km as being caused mainly by temperature variations of up to 300 K across the TTZ. Given that we found no large-scale temperature variations in the MTZ across the TTZ, the difference must be a feature mainly of the upper mantle. Assuming that the MTZ is more or less flat below central and eastern Europe, Ps delay times of the MTZ conversions could be used to investigate the upper mantle by Ps tomography (for  $V_p/V_s$  variations).

According to our results, the MTZ below the eastern Alps and the Carpathians seems to be thicker by up to 20 km, which confirms the results obtained from tomography studies (e.g. Piromallo *et al.* 2001; Piromallo & Facenna 2004). It seems probable that the thickening is real and not the effect of an anomalous  $V_p/V_s$  ratio in the mantle transition zone, because such large velocity differences are not observed in tomography studies. The MTZ thickening beneath the eastern Alps, the Pannonian Basin and the Carpathians is, therefore, comparable to that observed in the active subduction in Japan (Tonegawa *et al.* 2006,  $\sim 30 \text{ km}$ ). It may be that large flat slabs rest in the transition zone, similar to the case reported in Japan. Surprisingly, similar effects were not observed beneath Tibet, where the mantle transition zone seems to be of normal thickness (Yuan *et al.* 1997; Kind *et al.* 2002). This might point to different depth extents of collisional tectonics.

## ACKNOWLEDGMENTS

We thank our colleagues from the SZGRF Erlangen, the GRSN, GEOFON, IG CAS Prague, ReNaSS, ZAMG Vienna, PAN Warsaw, Bratislava, Hungary, Zurich and MedNet for providing data.

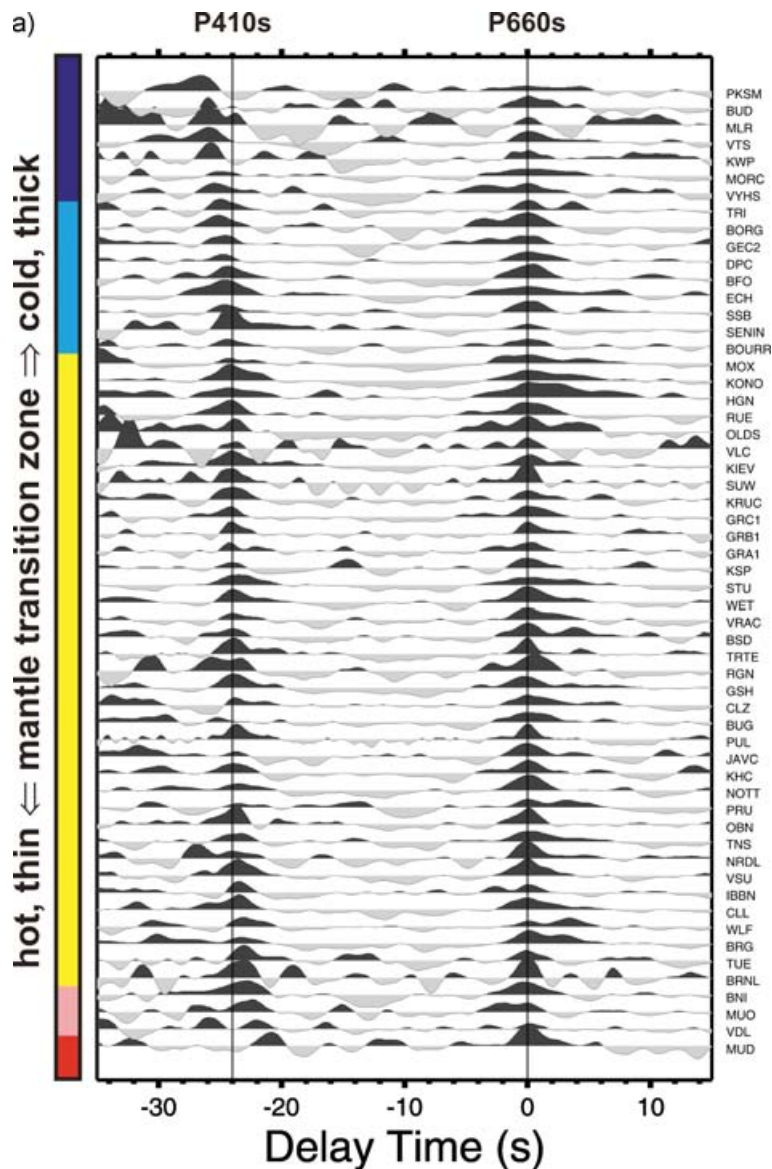


**Figure 13.** (a) Ps converted phases of the mantle transition zone aligned (and shifted) after the arrival time of the conversion from the 660 km discontinuity, showing differences in the thickness of the mantle transition zone. Several stations in the western Alps and MUD in Denmark, show reduced differential delay times, whereas most of the enlarged delay times are observed at stations in the area of the eastern Alps and the Carpathian belt. (b)  $P_{410s}$  delay times versus differential delay time ( $t_{P660s} - t_{P410s}$ ) for sum traces of single stations from (a). Almost all stations are within  $23.8 \pm 1$  s differential time. Stations in the EEC cluster at a delay time of 42.5 s for the 410 conversion and a differential time of 24 s, which implies a normal transition zone thickness but several per cent higher seismic velocities in the upper mantle than in the IASP91 standard earth model. There is perceptively less scattering in the EEC than in central Europe, which indicates that structure of the upper mantle beneath central Europe is more complicated than in the EEC. The trend defined by most stations from fast to slow upper mantle (smaller to larger  $P_{410s}$  delay times) confirms the trend already observed by Chevrot *et al.* (1999) for stations distributed worldwide.

Most data were obtained from SZGRF, GEOFON and IRIS data centres. This research was supported by the Deutsche Forschungsgemeinschaft and the EU project NERIES. We used the software packages SeismicHandler (Stammler 1993) and GMT (Wessels & Smith 1998) for most of the data processing and plotting.

## REFERENCES

- Alinaghi, A., Bock, G., Kind, R., Hanka, W. & Wylegalla, K., 2003. Receiver function analysis of the crust and upper mantle from the North German Basin to the Archaean Baltic Shield, *Geophys. J. Int.*, **155**, 641–652.
- Artemieva, I.M., 2003. Lithospheric structure, composition, and thermal regime of the East European craton: implications for the subsidence of the Russian platform, *Earth planet. Sci. Lett.*, **213**, 431–446.
- Banka, D., Pharaoh, T.C., Williamson, J.P. & TESZ Project Potential Field Core Group, 2002. Potential field imaging of Palaeozoic orogenic structure in northern and central Europe, *Tectonophysics*, **360**, 23–45.
- Benz, H.M. & Vidale, J.E., 1993. Sharpness of upper-mantle discontinuities determined from high-frequency reflections, *Nature*, **365**, 147–150.
- Bina, C.R. & Helffrich, G., 1994. Phase transition Clapeyron slopes and transition zone seismic discontinuity topography, *J. geophys. Res.*, **99**(B8), 15 853–15 860.
- Budweg, M., Bock, G. & Weber, M., 2006. The Eifel Plume—imaged with converted seismic waves, *Geophys. J. Int.*, **166**(2), 579–589, doi:10.1111/j.1365-246X.2005.02778.x.

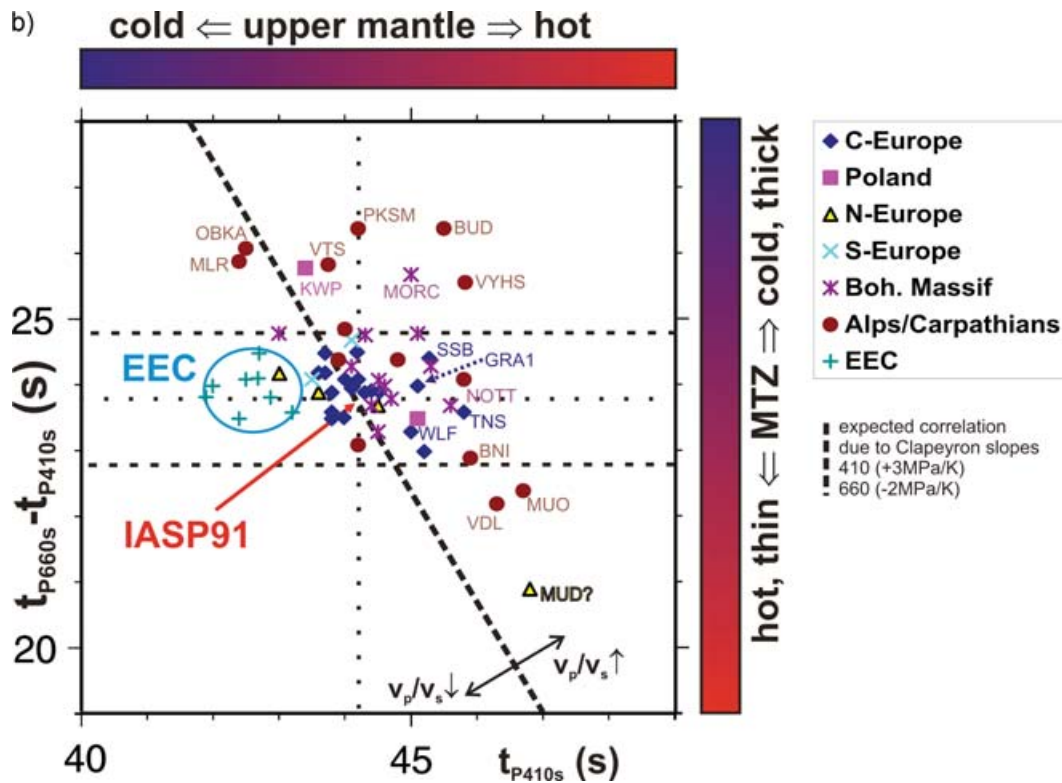


Figure 13. (Continued.)

- Chevrot, S., Vinnik, L.P. & Montagner, J.-P., 1999. Global-scale analysis of the mantle Pds phases, *J. geophys. Res.*, **104**(B9), 20 203–20 219.
- Cotte, N., Pedersen, H.A. & TOR Working Group, 2002. Sharp contrast in lithospheric structure across the Sorgenfrei-Tornquist Zone as inferred by Rayleigh wave analysis of TOR1 project data, *Tectonophysics*, **360**, 75–88.
- Deuss, A., Redfern, S.A.T., Chambers, K. & Woodhouse, J.H., 2006. The nature of the 660-kilometer discontinuity in Earth's mantle from global seismic observations of PP precursors, *Science*, **311**, 198–201.
- Dezes, P., Schmid, S.M. & Ziegler, P.A., 2004. Evolution of the European Cenozoic Rift System: interaction of the Alpine and Pyrenean orogens with their foreland lithosphere, *Tectonophysics*, **389**, 1–33.
- Fei, Y. *et al.*, 2004. Experimentally determined postspinel transformation boundary in  $Mg_2SiO_4$  using MgO as an internal pressure standard and its geophysical implications, *J. geophys. Res.*, **109**, B02305, doi:10.1029/2003JB002562.
- Geissler H. *et al.*, 2005. Seismic location of a  $CO_2$  source in the upper mantle of the western Eger rift, Central Europe, *Tectonics*, **24**, doi:10.1029/2004TC001672.
- Giiese, P., 1995. Main features of geophysical structures in central Europe, in *Pre-Permian Geology of Central and Eastern Europe*, eds R.D. Dallmeyer, W. Franke & K. Weber, pp. 7–25. Springer-Verlag, Berlin Heidelberg.
- Goes, S., Govers, R. & Vacher, P., 2000. Shallow upper mantle temperatures under Europe from P and S wave tomography, *J. geophys. Res.*, **105**, 11 153–11 169.
- Gossler, J. & Kind, R., 1996. Seismic evidence for very deep roots of continents, *Earth planet. Sci. Lett.*, **138**, 1–3.
- Grad M., Keller G.R., Thybo H., Guterch A. & POLONAISE Working Group, 2002. Lower lithospheric structure beneath the Trans-European Suture Zone from POLONAISE'97 seismic profiles, *Tectonophysics*, **360**, 153–168, doi:10.1016/S0040-1951(02)00350-5.
- Grunewald, S., Weber, M., & Kind, R., 2001. The upper mantle under Central Europe—indications for the Eifel plume, *Geophys. J. Int.*, **147**, 590–601.
- Hacker, B.R. & Abers, G.A., 2004. Subduction Factory 3: an Excel worksheet and macro for calculating the densities, seismic wave speeds, and  $H_2O$  contents of minerals and rocks at pressure and temperature, *Geochem. Geophys. Geosyst.* **G3**, **5**(1), Q01005, doi:10.1029/2003GC000614.
- Helfrich, G.R. & Wood, B.J., 1996. 410 km discontinuity sharpness and the form of the olivine-phase diagram: resolution and apparent seismic contradictions, *Geophys. J. Int.*, **126**, F7–F12.
- Helfrich, G.R. & Wood, B.J., 2001. The Earth's mantle, *Nature*, **412**, 501–507.
- Katsura, T. *et al.*, 2004. Olivine-wadsleyite transition in the system  $(Mg,Fe)_2SiO_4$ , *J. geophys. Res.*, **109**(B2), B02209, doi:10.1029/2003JB002438.
- Kennett, B.L.N., 1991. *IASP 1991 Seismological Tables*, Research School of Earth Sciences, Australian National University, Canberra, Australia.
- Kind, R., 1985. The reflectivity method for different source and receiver structures and comparison with GRF data, *J. Geophys.*, **58**, 146–152.
- Kind, R. & L.P. Vinnik, 1988. The upper-mantle discontinuities underneath the GRF array from P-to-S converted phases, *J. Geophys.*, **62**, 138–147.
- Kind, R., Kosarev, G.L. & Petersen, N.V., 1995. Receiver functions at the stations of the german regional seismic network (GRSN), *Geophys. J. Int.*, **121**, 191–202.
- Kind, R., Sobolev, S.V., Yuan, X., Li, X., Gossler, J. & Kosarev, G., 2000. Analysis of major global tectonic structures using P-to-S converted seismic wave, in *Problems in Geophysics for the New Millennium*, eds E. Boschi, G. Ekström & A. Morelli, pp. 141–150. Istituto Nazionale di Geofisica e Vulcanologia, Editrice Compositori, Bologna.
- Kind, R. *et al.*, 2002. Seismic images of crust and upper mantle beneath Tibet: evidence for Eurasian plate subduction, *Science*, **298**, 1219–1221.
- Kobussen, A.F., Cristensen, N.I. & Thybo, H., 2006. Constraints on seismic velocity anomalies beneath the Siberian craton from xenoliths and petrophysics, *Tectonophysics*, **425**, 123–135.

- Kopylova, M.G., Lo, J. & Christensen, N.I., 2004. Petrological constraints on seismic properties of the Slave upper mantle (Northern Canada), *Lithos*, **77**, 493–510.
- Kukkonen, I.T. & Peltonen, P., 1999. Xenolith-controlled geotherm for the central Fennoscandian Shield: implications for lithosphere-asthenosphere relations, *Tectonophysics*, **304**, 301–315.
- Lawrence, J.F. & Shearer, P.M., 2006. A global study of transition zone thickness using receiver functions, *J. geophys. Res.*, **111**, B06307, doi:10.1029/2005JB003973.
- Lebedev, S., Chevrot, S. & Van Der Hilst, R. D., 2002. Seismic evidence for Olivine phase changes at the 410- and 660-kilometer discontinuities, *Science*, **296**, 1300–1302.
- Lebedev, S., Chevrot, S. & Van Der Hilst, R. D., 2003. Correlation between the shear-speed structure and thickness of the mantle transition zone, *Phys. Earth planet. Inter.*, **136**, 25–40.
- Li, A., Fisher, K.M., Van Der Lee, S., Wysession, M.E. & Clarke, T.J., 1998. Mantle discontinuities and temperature under the North American continental keel, *Nature*, **395**, 160–163.
- Li, X., Kind, R. & Yuan, X., 2003a. Seismic study of upper mantle and transition zone beneath hotspots, *Phys. Earth. planet. Inter.*, **136**, 79–92.
- Li, X., Kind, R., Yuan, X., Sobolev, S.V. & Hanka, W., 2003b. Seismic observation of narrow plumes in the oceanic upper mantle, *Geophys. Res. Lett.*, **30**(4), 1334, doi:10.1029/2002GL015411.
- Lueschen, E., Borrini, D., Gebrande, H., Lammerer, B., Millahn, K., Neubauer, F., Nicolich, R., 2006. TRANSALP—deep crustal Vibroseis and explosive seismic profiling in the Eastern Alps, *Tectonophysics*, **414**, 9–38, doi:10.1016/j.tecto.2005.10.014.
- Meier, T., Malischewsky, P.G. & Neunhöfer, H., 1997. Reflection and transmission of surface waves at a vertical discontinuity and imaging of lateral heterogeneity using reflected fundamental rayleigh waves, *Bull. seism. Soc. Am.*, **87**(6), 1648–1661.
- Melbourne, T. & Helmberger, D., 1998. Fine structure of the 410-km discontinuity, *J. geophys. Res.*, **103**(B5), 10 091–10 102.
- Nemcok, M., Pospisil, L., Lexa, J., Donelick, R.A., 1998. Tertiary subduction and slab break-off model of the Carpathian-Pannonian region, *Tectonophysics*, **295**, 307–340.
- Niu, F. & Kawakatsu, H., 1996. Complex structure of the mantle discontinuities at the tip of the subducting slab beneath the northeast China: a preliminary investigation of broadband receiver functions, *J. Phys. Earth*, (J-array special issue), **44**, 701–711.
- Piomallo, C. & Facenna, C., 2004. How deep we can find the traces of Alpine subduction? *Geophys. Res. Lett.*, **31**, L06605, doi:10.1029/2003GL019288.
- Piomallo, C., Vincent, A.P., Yuen, D.A. & Morelli, A., 2001. Dynamics of the transition zone under Europe inferred from wavelet cross-spectra of seismic tomography, *Phys. Earth planet. Inter.*, **125**, 125–139.
- Priestley, K. & McKenzie, D., 2006. The thermal structure of the lithosphere from shear wave velocities, *Earth planet. Sci. Lett.*, **244**, 285–301.
- Ramesh, D.S., Kind, R. & X. Yuan, 2002. Receiver function analysis of the North American crust and upper mantle, *Geophys. J. Int.*, **150**, 91–108.
- Revenaugh, J. & Jordan T.H., 1991. Mantle Layering from ScS Reverberations. 2, The Transition Zone, *J. geophys. Res.*, **96**, 19 763–19 780.
- Ritzwoller, M.H., Shapiro, N.M., Barmin, M.P. & Levshin, A.L., 2002. Global surface wave diffraction tomography, *J. geophys. Res.*, **107**(B12), 2335.
- Shapiro, N.M. & Ritzwoller, M.H., 2002. Monte-Carlo inversion for a global shear velocity model of the crust and upper mantle, *Geophys. J. Int.*, **151**, 88–105, doi:10.1046/j.1365-246X.2002.01742.x.
- Shearer, P.M., 1990. Seismic imaging of upper mantle structure with new evidence for a 520-km discontinuity, *Nature*, **344**, 121–126.
- Seghedi, I., Downes, H., Harangi, S., Mason, P.R.D. & Pecskey, Z., 2005. Geochemical response of magmas to Neogene-Quaternary continental collision in the Carpathian-Pannonian region: a review, *Tectonophysics*, **410**, 485–499.
- Shearer, P.M., 2000. Upper mantle seismic discontinuities, in Earth's Deep Interior: Mineral Physics and Tomography from the Atomic to the Global Scale, *AGU Geophysical Monograph*, **117**, 115–131.
- Simmons, N.A. & Gurrrola, H., 2000. Multiple seismic discontinuities near the base of the transition zone in the Earth's mantle, *Nature*, **405**, 559–562.
- Smyth, J.R. & Frost, D.J., 2002. The effect of water on the 410-km discontinuity: an experimental study, *Geophys. Res. Lett.*, **29**(10), 1485, doi:10.1029/2001GL014418.
- Sperner, B., Lorenz, F., Bonjer, K., Hettel, S., Müller, B. & Wenzel, F., 2001. Slab break-off—abrupt cut or gradual detachment? New insights from the Vrancea Region (SE Carpathians, Romania), *Terra Nova*, **13**, 172–179.
- Stammler, K., 1993. SeismicHandler: programmable multichannel data handler for interactive and automatic processing of seismological analyses, *Comp. Geosci.*, **19**, 135–140.
- Stammler, K., Kind, R., Petersen, N., Kosarev, G., Vinnik, L. & Qiyuan, L., 1992. The upper mantle discontinuities: correlated or anticorrelated? *Geophys. Res. Lett.*, **19**, 1563–1566.
- Świczak, M., Grad, M., TOR & SVEKALAPKO Working Group, 2004. Upper mantle seismic discontinuities topography variations beneath Eastern Europe, *Act. Geophys. Pol.*, **52**(3), 251–270.
- Tonegawa, T., Hirahara, K., Shibutani, T. & Shiomi, K., 2006. Upper mantle imaging beneath the Japan Islands by Hi-net tiltmeter recordings, *Earth Planets Space*, **58**, 1007–1012.
- Tornquist, A., 1908. Die Feststellung des Süwestrandes des baltisch-russischen Schildes und die geotektonische Zugehörigkeit der ostpreussischen Scholle, *Schr. d. Phys.-ökon. Ges., Königsberg*, **49**(1), 1–12.
- TRANSALP Working Group, 2002. First deep seismic reflection images of the Eastern Alps reveal giant crustal wedges and transcrustal ramps, *Geophys. Res. Lett.*, **29**(10), doi:10.1029/2002GL014911.
- Van Der Lee, S., Paulssen, H. & Nolet, G., 1994. Variability of P660s phases as a consequence of topography of the 660 km discontinuity, *Phys. Earth planet. Inter.*, **86**, 147–164.
- van der Meijde, M., Marone, F., Giardini, D. & van der Lee, S., 2003. Seismic evidence for water deep in Earth's upper mantle, *Science*, **6**, **300**(5625), 1556–1558, doi:10.1126/science.1083636.
- Vacher, P., Mocquet, A. & Sotin, C., 1998. Computation of seismic profiles from mineral physics: the importance of the non-olivine components for explaining the 660 km depth discontinuity, *Phys. Earth planet. Int.*, **106**, 275–298.
- Vinnik, L.P., 1977. Detection of waves converted from P to S in the mantle, *Phys. Earth planet. Inter.*, **15**, 39–45.
- Wessels, P. & Smith, W.H.F., 1998. New, improved version of generic mapping tools released, *EOS Trans. Am. Geophys. Union*, **79**, 579.
- Wood, B.J., 1995. The effect of H<sub>2</sub>O on the 410-kilometer seismic discontinuity, *Science*, **268**, 74–76.
- Wortel, M.J.R. & Spakman, W., 2000. Subduction and slab detachment in the mediterranean-carpathian region, *Science*, **290**, 1910–1917.
- Yegorova, T.P. & Starostenko, V.I., 1999. Large-scale 3D gravity analysis of the lithosphere below the transition zone from Western Europe to East-European platform, *Tectonophysics*, **314**, 83–100.
- Yuan, X., Ni, J., Kind, R., Mechie, J. & Sandvol, E., 1997. Lithospheric and upper mantle structure of southern Tibet from a seismological passive source experiment, *J. geophys. Res.*, **102**(B12), 27 491–27 500.
- Zandt, G., Myers, S.C. & Wallace, T.C., 1995. Crust and mantle structure across the Basin and Range-Colorado Plateau boundary at 37°N latitude and implications for Cenozoic extensional mechanism, *J. geophys. Res.*, **100**(B6), 10 529–10 548.
- Zhu, L. & Kanamori, H., 2000. Moho depth variation in southern California from teleseismic receiver functions, *J. geophys. Res.*, **105**(B2), 2969–2980.
- Zielhuis, A. & Nolet, G., 1994. Shear-wave variations in the upper mantle beneath Central Europe, *Geophys. J. Int.*, **117**, 695–715.

## APPENDIX A

By analysing 25 yr of data from station GRA1 (1980–2004) for each year separately, variations in the Moho Ps delay times of 0.1 s could be observed (see Table A1). Therefore, the uncertainty of Moho Ps delay time measurements for temporary stations, which were operated for 1 yr, might also be in the range 0.1–0.2 s. Delay times  $t_{P410s}$  and  $t_{P660s}$ , observed in station stacks

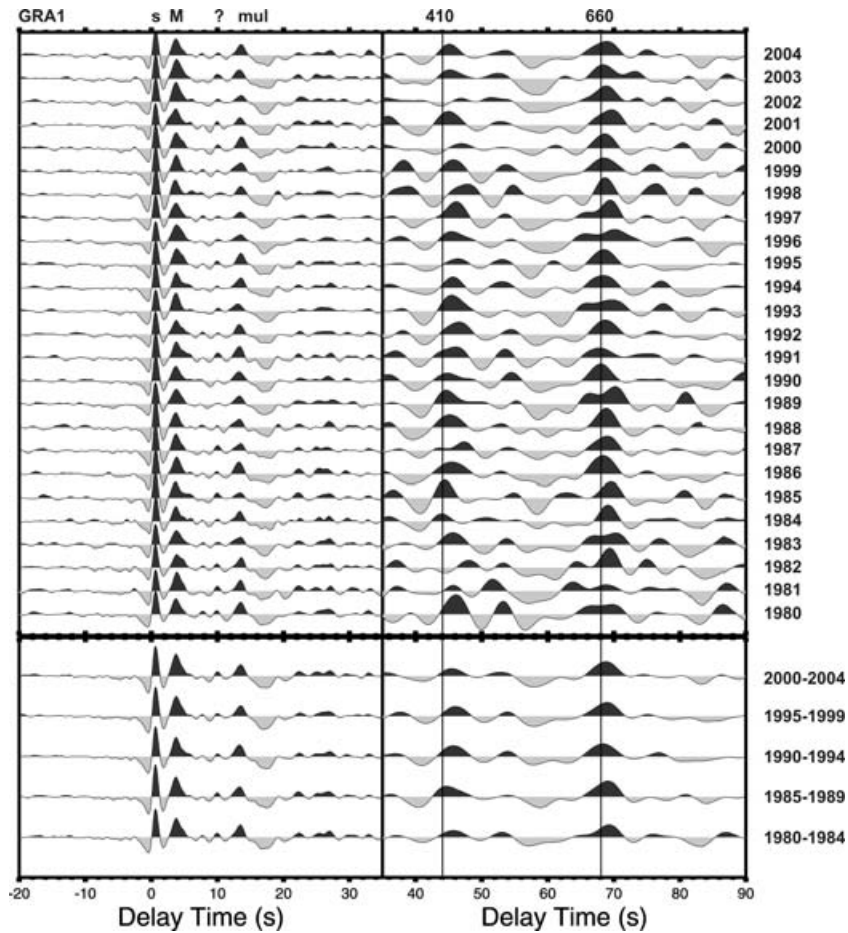


**Figure A1.** Stacked receiver functions from station GRA1 for every year between 1980 and 2004. Data were high-pass filtered with 50 s corner period in the time range  $-20$  to  $35$  s delay time and band-pass filtered (corner periods  $5-50$  s) from  $35$  to  $90$  s delay time, respectively (see also Fig. A2).

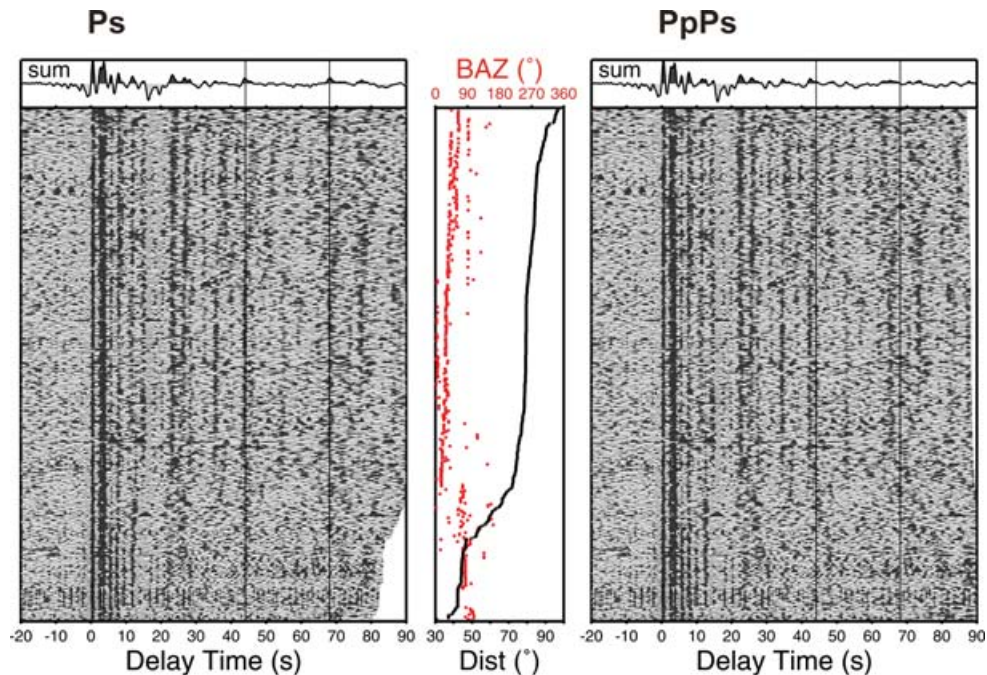


**Figure A2.** Single moveout-corrected traces for station GRB1 (backazimuth  $0-180^\circ$ , sorted by epicentral distance), corrected for primary Ps phases (left-hand side) and multiple phases PpPs (right-hand side). High-frequency multiple phases from crustal discontinuities can sometimes be observed up to delay times of at least  $50$  s. This may disturb the primary signal from the  $410$  km discontinuity in single traces, as well as in the narrow backazimuth bins that are used for stacking common conversion points.

**Table A1.** Table with results from stacking of receiver functions from different years for station GRA1.

Year	Moho (HP 50s)				MTZ (BP 3s-50s)				MTZ (BP 5s-50s)				MTZ (HP 50s)				
	$V_p/V_s$	$H$ (km)	$t_{PMs}$ (s)	$A_{Moho}$	$n$	$t_{P410s}$ (s)	$t_{P660s}$ (s)	$df_{660-410}$ (s)	$t_{P410s}$ (s)	$t_{P660s}$ (s)	$df_{660-410}$ (s)	$t_{P410s}$ (s)	$t_{P660s}$ (s)	$df_{660-410}$ (s)	$t_{P410s}$ (s)	$t_{P660s}$ (s)	$df_{660-410}$ (s)
1980	1.73	31.5	3.7	0.10	38	46.7	69.7	23.0	46.1	69.7	23.6	44.8; 46.8	69.8		44.8; 46.8	69.8	26
1981	1.76	31.0	3.9	0.12	35	45.7	70.1/67.7		45.7	68.8	23.1	45.1; 46.5	67.6; 70.1		45.1; 46.5	67.6; 70.1	32
1982	1.74	31.5	3.8	0.09	29	48.7	69.6	20.9	48.0	69.4	21.4	48.8	69.5	20.7	48.8	69.5	28
1983	1.71	32.0	3.8	0.09	39	45.4	70.8	25.4	45.6	70.3	24.7	45.2	70.6	25.4	45.2	70.6	35
1984	1.73	31.5	3.7	0.10	45	44.7	69.3	24.6	43.9	69.1	25.2	44.9	69.5	24.6	44.9	69.5	43
1985	1.70	32.0	3.7	0.10	43	44.6	70.0	25.4	44.4	69.6	25.2	44.8	68.8; 70.2		44.8	68.8; 70.2	37
1986	1.76	31.0	3.8	0.11	41	44.4	69.1	24.7	45.5	68.4	22.9	44.9; 47.0	69.0		44.9; 47.0	69.0	39
1987	1.73	31.5	3.7	0.11	55	47.3	69.5	22.2	47.4	69.0	21.6	46.9	68.8	21.9	46.9	68.8	52
1988	1.72	31.5	3.7	0.10	39	44.7	69.2	24.5	45.1	68.8	23.7	44.7	69.4	24.7	44.7	69.4	35
1989	1.73	31.5	3.8	0.10	39	44.5	70.2	25.7	44.6	70.2	25.6	44.8	70.3	25.5	44.8	70.3	37
1990	1.73	31.5	3.7	0.10	50	45.0	68.3	23.3	44.8	68.0	23.2	44.5	68.3	23.8	44.5	68.3	44
1991	1.73	31.5	3.8	0.10	46	47.0	68.7	21.7	46.1	67.8	21.7	45.1; 47.3	69.0		45.1; 47.3	69.0	43
1992	1.73	31.5	3.7	0.09	62	44.5/47.3	69.4		46.6	68.7	22.1	44.4; 47.2	69.5		44.4; 47.2	69.5	59
1993	1.73	31.5	3.7	0.12	43	45.2	68.4	23.2	45.5	69.7	24.2	45.1	68.3; 71.3		45.1	68.3; 71.3	38
1994	1.71	32.0	3.8	0.10	64	45.4	69.0	23.6	45.7	68.4	22.7	45.0	68.7	23.7	45.0	68.7	56
1995	1.74	31.5	3.8	0.11	58	47.4	69.2	21.8	46.4	68.5	22.1	45.0; 47.1	69.2		45.0; 47.1	69.2	48
1996	1.74	31.5	3.8	0.11	47	45.3	69.8	24.5	45.4	70.1	24.7	45.1	69.7	24.6	45.1	69.7	41
1997	1.72	31.5	3.7	0.10	38	46.4	69.6	23.2	46.2	69.5	23.3	46.6	69.4	22.8	46.6	69.4	31
1998	1.68	32.0	3.6	0.10	26	45.4	68.3	22.9	47.8	68.7	20.9	45.2; 47.6	68.4		45.2; 47.6	68.4	20
1999	1.73	31.5	3.8	0.11	42	45.1	68.2	23.1	45.0	68.5	22.8	44.9	68.3	23.4	44.9	68.3	35
2000	1.71	32.0	3.7	0.10	40	45.2	69.1	23.9	46.9	68.7	21.8	44.9	69.0	24.1	44.9	69.0	31
2001	1.71	31.5	3.7	0.11	36	44.2	66.9/70.0		45.0	69.7	24.7	44.5	69.5	25.0	44.5	69.5	34
2002	1.70	32.5	3.7	0.13	35	47.3	68.7	21.4	46.9	68.9	22.0	47.2	69.0	21.8	47.2	69.0	33
2003	1.73	31.5	3.8	0.13	49	44.6	69.5	24.9	45.1	68.4	23.3	44.8	68.6; 69.9		44.8	68.6; 69.9	44
2004	1.71	32.0	3.7	0.11	47	45.0	69.5	24.5	45.1	68.9	23.8	44.9	69.4	24.5	44.9	69.4	44
Mean	1.72	31.6	3.7	0.1	43	45.6	69.3	23.6	45.8	69.0	23.2	45.4	69.3	23.8	45.4	69.3	39
$\sigma$	0.02	0.3	0.1	0.0	9	1.2	0.6	1.4	1.0	0.7	1.3	1.2	0.6	1.4	1.2	0.6	9
1980-1984	1.73	31.5	3.8	0.10	176	45.3	69.5	24.2	45.7	69.3	23.6	45.0	69.6	24.6	45.0	69.6	164
1985-1989	1.73	31.5	3.7	0.10	217	44.5	69.6	25.1	44.7	69.1	24.4	44.7	69.7	25.0	44.7	69.7	200
1990-1994	1.73	31.5	3.7	0.10	265	45.2	68.7	23.5	45.7	68.4	22.7	44.9	68.6	23.7	44.9	68.6	240
1995-1999	1.73	31.5	3.8	0.10	211	45.4	69.3	23.9	46.0	69.0	23.0	45.0	69.3	24.3	45.0	69.3	175
2000-2004	1.73	31.5	3.7	0.11	207	44.9	69.4	24.5	45.4	68.8	23.4	44.8	69.4	24.6	44.8	69.4	186
Mean	1.73	31.5	3.7	0.10	215	45.1	69.3	24.2	45.5	68.9	23.4	44.9	69.3	24.4	44.9	69.3	193
$\sigma$	0.0	0.0	0.1	0.01	32	0.4	0.4	0.6	0.5	0.3	0.6	0.1	0.4	0.5	0.1	0.4	29
1980-2004	1.73	31.5	3.7	0.10	1093	45.0	69.3	24.3	45.6	68.8	23.2	44.9	69.4	24.5	44.9	69.4	980

**Table A2.** Parameters of seismic velocity models used to calculate synthetic receiver functions.

Depth (km)	$V_p$ (km s <sup>-1</sup> )	$V_s$ (km s <sup>-1</sup> )	rho (g cm s <sup>-3</sup> )	$Q_p$	$Q_s$	$n$ (layers)
<b>(a) IASP91 reference model (Kennett 1991).</b>						
0	5.8	3.36	2.8	1350	600	0
10	5.8	3.36	2.8	1350	600	1
20	5.8	3.36	2.8	1350	600	1
20	6.5	3.75	3	1350	600	0
35	6.5	3.75	3	1350	600	1
35	8.04	4.47	3.38	1350	600	0
71	8.044	4.483	3.37688	1447	600	4
120	8.05	4.5	3.37091	195	80	8
171	8.192	4.51	3.3671	195	80	5
210	8.3	4.518	3.4	195	80	5
210	8.3	4.522	3.4	362	143	0
271	8.523	4.628	3.46264	365	143	6
371	8.888	4.802	3.51639	370	143	10
410	9.03	4.87	3.54325	372	143	5
410	9.36	5.07	3.72378	366	143	0
450	9.494	5.1548	3.78678	365	143	8
500	9.662	5.2608	3.8498	364	143	8
550	9.83	5.3668	3.91282	363	143	8
600	9.9984	5.4728	3.97584	362	143	8
635	10.116	5.547	3.98399	362	143	6
660	10.2	5.6	3.99214	362	143	6
660	10.79	5.95	4.38071	759	312	0
721	10.9521	6.1083	4.41241	744	312	10
771	11.0756	6.218	4.44316	730	312	8
871	11.2506	6.2929	4.50372	737	312	15
<b>(b) BM3A (BM, Bohemian Massif)</b>						
0	5.4	3.12	2.6	1350	600	5
4	6	3.47	2.7	1350	600	5
11	6.2	3.58	2.8	1350	600	5
13	6.3	3.64	2.8	1350	600	5
25	6.3	3.64	2.8	1350	600	5
34	8	4.47	3	1350	600	5
71	8.044	4.483	3.37688	1447	600	4
71	7.785	4.21	3.37091	195	80	0
100	7.785	4.21	3.37091	195	80	8
120	7.785	4.21	3.37091	195	80	8
171	7.785	4.21	3.3671	195	80	5
210	7.785	4.21	3.3671	195	80	5
210	8.3	4.522	3.4	362	143	0
271	8.523	4.628	3.46264	365	143	6
371	8.888	4.802	3.51639	370	143	10
410	9.03	4.87	3.54325	372	143	5
410	9.36	5.07	3.72378	366	143	0
450	9.494	5.1548	3.78678	365	143	8
500	9.662	5.2608	3.8498	364	143	8
550	9.83	5.3668	3.91282	363	143	8
600	9.9984	5.4728	3.97584	362	143	8
635	10.116	5.547	3.98399	362	143	6
660	10.2	5.6	3.99214	362	143	6
660	10.79	5.95	4.38071	759	312	0
721	10.9521	6.1083	4.41241	744	312	10
771	11.0756	6.218	4.44316	730	312	8
871	11.2506	6.2929	4.50372	737	312	15
<b>(c) EEC4D (EEC, East European Craton)</b>						
20	6.5	3.757	2.8	1350	600	5
30	6.8	3.931	3	1350	600	5
50	7.1	4.104	3	1350	600	5
50	8.1	4.628	3.3	1350	600	0
71	8.144	4.654	3.30688	1447	600	4
120	8.15	4.657	3.32091	1447	600	8
171	8.192	4.681	3.3671	1447	600	5
<b>(d) BM1A (BM, Bohemian Massif)</b>						
0	5.4	3.12	2.6	1350	600	5
4	6	3.47	2.7	1350	600	5
11	6.2	3.58	2.8	1350	600	5
13	6.3	3.64	2.8	1350	600	5
25	6.3	3.64	2.8	1350	600	5
34	8	4.47	3	1350	600	5
71	8.044	4.483	3.37688	1447	600	4
71	7.785	4.35	3.37091	195	80	0
100	7.785	4.35	3.37091	195	80	8
120	7.785	4.35	3.37091	195	80	8
171	7.785	4.35	3.3671	195	80	5
210	7.785	4.35	3.3671	195	80	5
210	8.3	4.522	3.4	362	143	0
271	8.523	4.628	3.46264	365	143	6
371	8.888	4.802	3.51639	370	143	10
410	9.03	4.87	3.54325	372	143	5
410	9.36	5.07	3.72378	366	143	0
450	9.494	5.1548	3.78678	365	143	8
500	9.662	5.2608	3.8498	364	143	8
550	9.83	5.3668	3.91282	363	143	8
600	9.9984	5.4728	3.97584	362	143	8
635	10.116	5.547	3.98399	362	143	6
660	10.2	5.6	3.99214	362	143	6
660	10.79	5.95	4.38071	759	312	0
721	10.9521	6.1083	4.41241	744	312	10
771	11.0756	6.218	4.44316	730	312	8
871	11.2506	6.2929	4.50372	737	312	15
<b>(e) EEC4C (EEC, East European Craton)</b>						
0	6	3.468	2.8	1350	600	0
10	6.3	3.641	2.8	1350	600	5
20	6.5	3.757	2.8	1350	600	5
30	6.8	3.931	3	1350	600	5
50	7.1	4.104	3	1350	600	5
50	8.04	4.47	3.3	1350	600	0
71	8.044	4.483	3.30688	1447	600	4
120	8.05	4.5	3.32091	1447	600	8
171	8.192	4.51	3.3671	1447	600	5
210	8.3	4.518	3.4	1447	600	5
210	8.3	4.522	3.4	362	143	0
271	8.523	4.628	3.46264	365	143	10
371	8.888	4.802	3.51639	370	143	10
410	9.03	4.87	3.54325	372	143	5
410	9.36	5.07	3.72378	366	143	0
450	9.494	5.1548	3.78678	365	143	8
500	9.662	5.2608	3.8498	364	143	8
550	9.83	5.3668	3.91282	363	143	8
600	9.9984	5.4728	3.97584	362	143	8

Depth (km)	$V_p$ (km s <sup>-1</sup> )	$V_s$ (km s <sup>-1</sup> )	rho (g cm s <sup>-3</sup> )	$Q_p$	$Q_s$	$n$ (layers)
635	10.116	5.547	3.98399	362	143	6
660	10.2	5.6	3.99214	362	143	6
660	10.79	5.95	4.38071	759	312	0
721	10.9521	6.1083	4.41241	744	312	10
771	11.0756	6.218	4.44316	730	312	8
871	11.2506	6.2929	4.50372	737	312	15

of GRA1 and OBN (no figure) for different years of observation, vary by about 0.5 (up to 1.0) s, showing no dependency on the filter used. It may therefore be assumed that the uncertainties for delay time measurements of conversions from the mantle transition zone (410 and 660) are also in the range 0.5–1.0 s for temporary stations. For many stations, absolute delay times for the 410 and 660 km discontinuities depend on the filter used (most obviously for the 410 conversion). This might be caused by higher-order crustal

reverberations, which may interfere with the primary 410 conversion (see Fig. A2).

In Fig. A2 we show single moveout-corrected traces of station GRB1 sorted by distance and moveout, corrected for primary conversions Ps (a) and multiple phases PpPs (b), respectively. It is obvious from frequency content and remaining moveout that multiple phases also exist at later Ps delay times, disturbing the primary signals of the 410 and 660 conversions. Theoretical receiver functions for the IASP91 earth model show beside primary conversions from the middle crust, Moho and mantle transition zone also strong multiple phases at around 30 s (Fig. 11a). In the sum trace of moveout-corrected traces this multiple phase is suppressed. If we have a real dataset with excellent distance coverage, multiple phases will be diminished during stacking. If we stack traces over small bins of distance and backazimuth, we will get a mixed signal of primary and multiple energy. This fact should be considered when stacking data for a common conversion point or interpreting migrated sections in detail.